AGU PUBLICATIONS

Geochemistry, Geophysics, Geosystems

RESEARCH ARTICLE

10.1002/2017GC007330

Key Points:
- SGD is the dominant source of nutrients to the Maowei Sea
- The SGD-derived nutrients are higher in the Maowei Sea than those estimated in other similar studies
- SGD-derived nutrients could support high-quantity aquaculture (oyster) in the Maowei Sea

Correspondence to:
J. Du,
jzdu@sklec.ecnu.edu.cn

Citation:
Chen, X., Lao, Y., Wang, J., Du, J., Liang, M., & Yang, B. (2018). Submarine groundwater-borne nutrients in a tropical bay (Maowei Sea, China) and their impacts on the oyster aquaculture. *Geochemistry, Geophysics, Geosystems*, *19*, 932–951. https://doi.org/10.1002/2017GC007330

Received 30 NOV 2017
Accepted 30 JAN 2018
Accepted article online 6 MAR 2018
Published online 30 MAR 2018

Submarine Groundwater-Borne Nutrients in a Tropical Bay (Maowei Sea, China) and Their Impacts on the Oyster Aquaculture

Xiaogang Chen[1], Yanling Lao[2,3], Jinlong Wang[1], Jinzhou Du[1], Mingzhong Liang[3], and Bin Yang[3]

[1]State Key Laboratory of Estuarine and Coastal Research, East China Normal University, Shanghai, China, [2]College of Resources and Environment, Qinzhou University, Qinzhou, China, [3]Guangxi Key Laboratory of Marine Disaster in the Beibu Gulf, Qinzhou University, Qinzhou, China

Abstract Submarine groundwater discharge (SGD) has been recognized as an important pathway for nutrients into estuaries, coasts, and the adjacent seas. In this study, ^{222}Rn was used to estimate the SGD-associated nutrient fluxes into an aquaculture area in a typical tropical bay (Maowei Sea, China). The SGD into the Maowei Sea during June 2016 was estimated to be 0.36 ± 0.33 m d^{-1} and was associated with SGD-derived dissolved inorganic nitrogen (DIN), dissolved inorganic phosphorus (DIP), and dissolved silicon (DSi) fluxes (mol d^{-1}) of $(4.5 \pm 5.5) \times 10^6$, $(5.3 \pm 9.1) \times 10^4$, and $(9.4 \pm 9.3) \times 10^6$, respectively. The SGD-derived nutrients (i.e., DIN, DIP, and DSi) were more than 1.9, 0.9, and 3.6 times the amounts in the local river input and served as dominant sources in the nutrient budgets in the Maowei Sea. Moreover, the N/P ratios in the SGD around the Maowei Sea were high (mean: 64), and these ratios likely exceeded the environmental self-purification capacity, thereby enhancing the biomass and changing the phytoplankton community structure. Therefore, SGD processes with derived nutrients may affect the biogeochemical cycles and marine ecological environment in the Maowei Sea. Furthermore, the N/P ratios ($\sim$67) in oysters are very close to those in the SGD in the Maowei Sea; this coincidence suggests that the high N/P ratios in the SGD are likely to be one of the most important sources that support oyster aquaculture, which might weaken the burden of water eutrophication in the Maowei Sea.

1. Introduction

Submarine groundwater discharge (SGD) is one of the most important and central processes of land-ocean interaction in coastal zones (LOICZ; Charette et al., 2012; Moore, 2010), and it defined as any or all fluid flow (including both terrestrial fresh groundwater and recirculated seawater) on continental margins from the seabed to the coastal ocean without regard to fluid composition or driving force (Burnett et al., 2003). SGD exhibits different geochemical properties (e.g., pH, Eh, and nutrient components) and can be modified by biogeochemical processes in coastal aquifers (Burnett et al., 2003; Slomp & Van Cappellen, 2004; Smith et al., 2008). Such processes involve the desorption of ions from adsorbed sites; dissolution and precipitation of carbonates; release of carbon, nutrients, and metals due to remineralization of organic matter; and oxidation-reduction reactions leading to the release or sequestration of other irons (Moore, 2010). However, nitrogen and phosphorus inputs from rivers and SGD could be enhanced by nutrients and other materials through natural processes or anthropogenic activities (e.g., fertilizer use and sewage discharge) in watersheds and coastal zones (Burnett et al., 1990; X. L. Wang et al., 2014). Generally, the major driving forces of rivers are climate change and human activities (Lu et al., 2011; Dai et al., 2013, 2016). However, the driving forces of SGD include terrestrial driving forces (mainly hydraulic gradients) and marine driving forces (such as tidal pumping, density gradients, waves, storms, and seabed topography; Zhang et al., 2016). These forces drive the groundwater discharge and drive nutrients into the sea. Because groundwater contains high nutrient concentrations, a small amount of SGD may transport a large quantity of nutrients (Boehm et al., 2006; Wu et al., 2013). Thus, SGD-derived nutrients may play a significant role in controlling water quality and can lead to associated deleterious effects on marine ecological environments (Ji et al., 2013; Wu, et al., 2013), such as red tide outbreaks (Hu et al., 2006; Lee et al., 2010; Luo & Jiao, 2016), benthic macroalgal eutrophication (Hwang et al., 2005), and hypoxia (McCoy et al., 2011).

Recent research has highlighted the significance of SGD as one of the most important pathways for the transport of dissolved materials from land to the ocean (Burnett & Dulaiova, 2006; Burnett et al., 1990, 2003; Su et al., 2011; Swarzenski et al., 2007). Three methods have been used to quantify the SGD in heterogeneous systems: physical measurements (seepage meters; e.g., Burnett & Dulaiova, 2006; Taniguchi et al., 2006), hydrogeological models (e.g., McCormack et al., 2014), and geochemical tracers (e.g., Burnett & Dulaiova, 2006; Huang et al., 2011; Swarzenski et al., 2007). In particular, naturally occurring radiotracers have been widely used to quantify SGD rates (Burnett & Dulaiova, 2006; Gu et al., 2012; Santos et al., 2015; Swarzenski et al., 2007). The main advantage of using naturally occurring radiotracers is that they present integrated signals related to different groundwater pathways in coastal aquifers (Burnett & Dulaiova, 2006). Radon (^{222}Rn, half-life 3.82 days) is a natural tracer that is widely enriched in groundwater relative to coastal seawater and is relatively easy to measure (Cable et al., 1996). Thus, ^{222}Rn serves as an excellent qualitative and quantitative tracer for identifying and quantifying groundwater inputs. Furthermore, continuous measurement of ^{222}Rn in seawater can be accomplished using a RAD7 electronic radon detector (Durridge Co. Inc., USA) together with a RAD-AQUA accessory (Burnett & Dulaiova, 2003).

Bay regions are the most sensitive land-ocean interaction area in coastal zones. Because of the influences of high human activity levels and high-intensity developments in watershed and coastal zones, bay regions have undergone unprecedented changes (Ge et al., 2014; Dai et al., 2014). The Maowei Sea is a typical tropical bay with high-intensity aquaculture activity where industrialization and urbanization have simultaneously changed the natural ecosystem structure and marine ecological environment (Gu et al., 2015; Zhang et al., 2014; Zheng et al., 2012; Li et al., 2017), especially in the Qinzhou Harbor area. Recently, the nitrogen, phosphate and chemical oxygen demand (COD) concentrations in the Maowei Sea have been reportedly increasing, and the tendency of eutrophication has been gradually aggravated (Lan & Peng, 2011). The abundance of some phytoplankton has reached levels of red tide occurrence in the Maowei Sea. For example, in March 2008, the biomass of *Skeletonema costatum* was 1.16×10^6 to 4.63×10^7 cells L^{-1} in the Maowei Sea (Zhuang et al., 2012). Nevertheless, our previous work reported that SGD-derived nutrient fluxes could not only support high densities of aquaculture activities but also reduce the impacts of N and P on local marine ecosystems in Sanggou Bay (X. L. Wang et al., 2014). Although environmental monitoring has been routinely conducted in the Maowei Sea since the 1980s (Lan & Peng, 2011; Wei et al., 2002), to the best of our knowledge, SGD and its derived nutrient fluxes have not been reported, which limits the understanding of the biogeochemical processes, environmental policy formulation, and environmental management in the Maowei Sea.

In this study, we combined automated radon and nutrient observations at a fixed station to obtain insight into how to quantify the tidally driven groundwater and nutrient fluxes via SGD in the Maowei Sea. Based on a ^{222}Rn mass balance model, we attempted to estimate the SGD by calculating the fluxes of all ^{222}Rn sources and sinks (Figure 1). The objectives of this work were to estimate the fluxes of SGD-associated nutrient inputs into the Maowei Sea, analyze the nutrient budgets, and evaluate the possible impacts of SGD-associated nutrient inputs on the coastal ecosystem.

2. Materials and Methods

2.1. Study Area

The Maowei Sea (surface area: ~135 km^2) belongs to the enclosed inner bay of Qinzhou Bay, which is located south of Qinzhou, in Guangxi Province and is adjacent to the Beibu Gulf (Figure 2a). The water depth ranges from 0.1 to 5 m, and the total coastline length is ~120 km in the Maowei Sea. As a semienclosed bay, the longitudinal length of this bay is ~15 km, and its mouth length is ~2 km (Figure 2b). The climate of this region is classified as a tropical maritime monsoon with a mean annual temperature of 22.1°C. The mean annual rainfall is 2,140 mm. In addition, the rainy season is between May and September (Tian et al., 2014). An irregular diurnal tide exists in this region, with a mean tidal range of 2.5 m and a maximum of 5.5 m (Editorial Board of China Bay Survey, 1993; Tian et al., 2014).

Two rivers (the Maolingjiang River and Qinjiang River) deliver 2.8×10^{10} m^3 yr^{-1} of fresh water and 8.6×10^4 t yr^{-1} of suspended sediment into the Maowei Sea (Wang, 2013). A mixed accumulation landform (delta) developed where the two rivers flow into the sea. The sediments gradually become coarser from the bayhead to the mouth of the Maowei Sea, changing from sandy mud near the bayhead to muddy sand in the middle of the bay then to fine sand and medium sand at the mouth of the Maowei Sea (Editorial Board

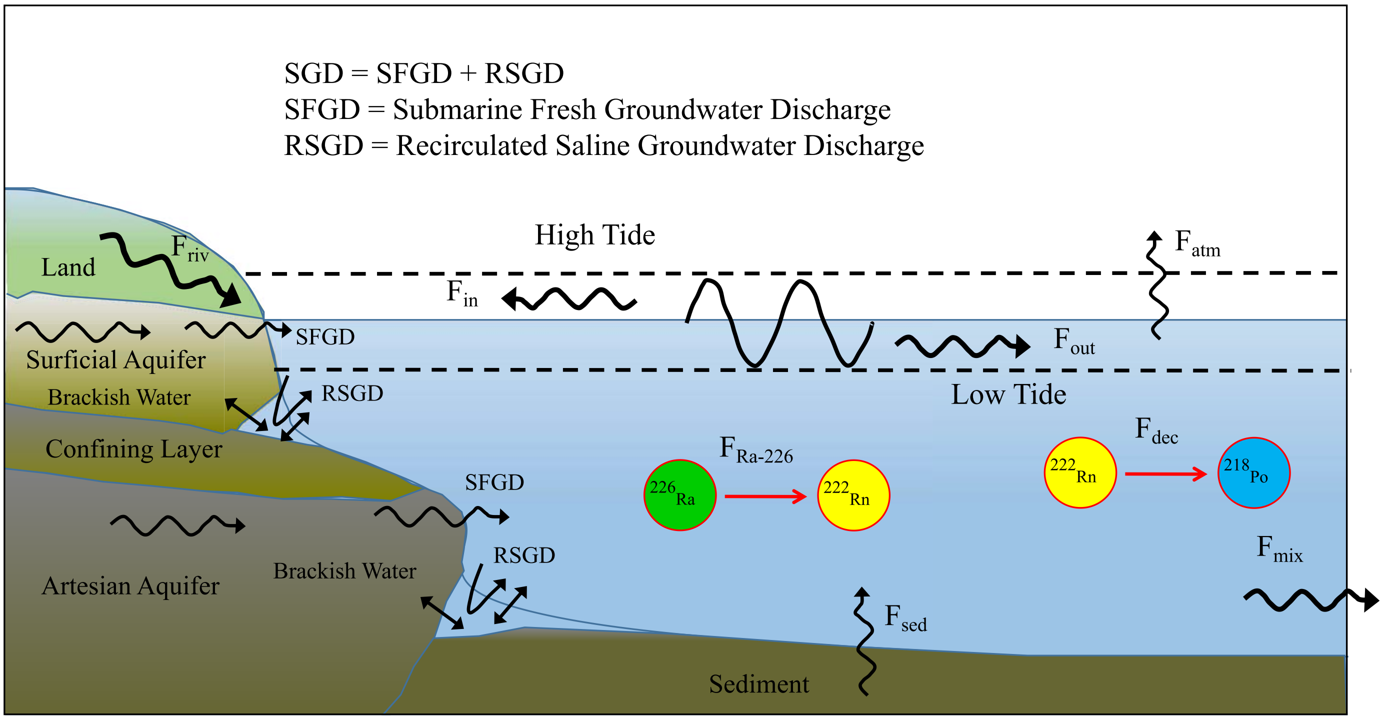

Figure 1. Schematic diagram of ^{222}Rn processes in the coastal zone (modified from Burnett & Dulaiova, 2003; Moore, 2010; Taniguchi et al., 2002). *Sources*: SGD input (F_{SGD}), river input (F_{riv}), influx during flood tides (F_{in}), ingrowth rate of dissolved ^{226}Ra in the water column ($F_{Ra\text{-}226}$), and diffusion flux from surface sediment into the water column (F_{sed}); sinks: outflux during ebb tides (F_{out}), atmospheric evasion (F_{atm}), decay loss of ^{222}Rn (F_{dec}), and mixing loss with offshore waters of ^{222}Rn (F_{mix}).

of China Bay Survey, 1993). The median diameter (D_{50}) of the sediments in the Maowei Sea is 0.334 mm (Wang, 2013).

The Maowei Sea is the largest natural oyster growing area (Wu et al., 2014) and the largest mangrove island in China. The distribution of aquaculture and mangroves in the Maowei Sea is shown in Figure 2c. However, as an important bay in the Beibu Gulf, the Maowei Sea has gradually become polluted because of human

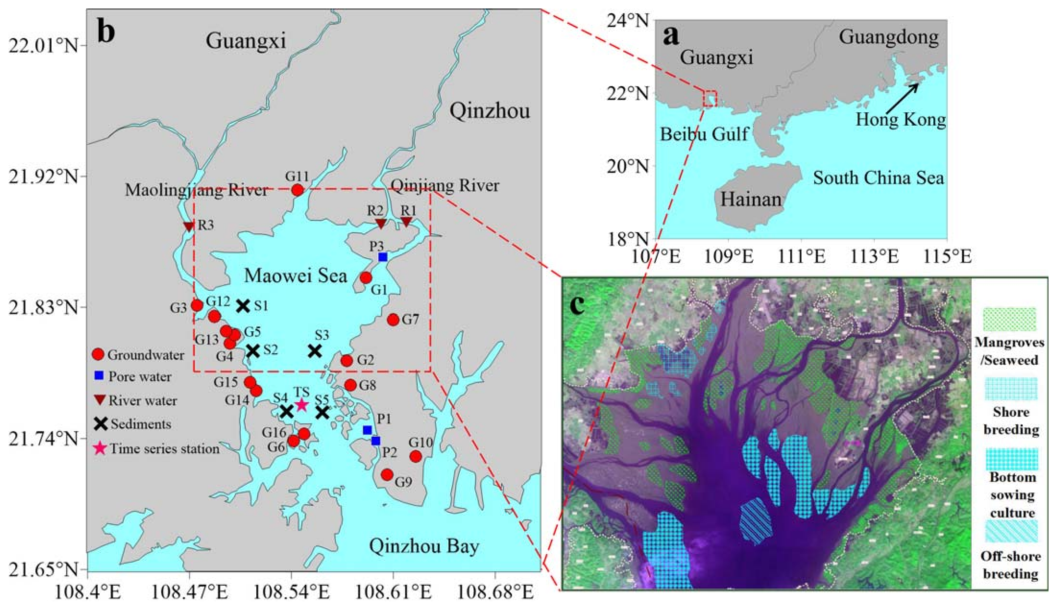

Figure 2. Map showing (a) the study site location, (b) sampling stations, and (c) the distribution of aquaculture and mangroves in the Maowei Sea.

activities, such as industrial wastewater discharge, daily municipal life, and agricultural fertilizer pollution (Editorial Board of China Bay Survey, 1993). These contaminants partly enter both the surface water and groundwater systems.

2.2. Sampling Strategy

2.2.1. Time Series Deployments

For continuous ^{222}Rn monitoring in seawater, a floating wooden building near the mouth of the Maowei Sea was used as a time series station (water depth: $\sim$5 m; Figure 3a). The water was continuously pumped into the RAD-AQUA system with a submersible pump that was fixed at 0.5 m above the seafloor. Continuous measurements of the ^{222}Rn in the seawater were measured in situ (Figure 3b) from 7:40 P.M. on 19 June 2016 to 9:40 P.M. on 20 June 2016. In parallel with the continuous ^{222}Rn monitoring, the water temperature and salinity were measured every 15 min using an YSI-EC300A conductivity meter placed near the submersible pump. The wind speed was measured every 15 min with a handheld anemometer. Nutrient samples were taken every 60 min and were subsequently analyzed in the lab. Fifty liters of surface water was collected every 3 h to observe the ^{226}Ra variation. A RAD7 detector was set up to automatically count every 30 min. The ^{222}Rn activity of the water was obtained by multiplying the ^{222}Rn activity of the air by the partition coefficient (α) when the ^{222}Rn in the air reached equilibrium with the ^{222}Rn in the water. The α was described by the Fritz Weigel equation (Burnett & Dulaiova, 2003) as follows:

$$\alpha = 0.105 + 0.405e^{-0.0502T} \tag{1}$$

where T is the water temperature (°C).

Figure 3. (a) The time series station was conducted in a floating wooden building and continuous ^{222}Rn was measured with a RAD7 Detector and RAD AQUA; (b) the salinity and temperature were determined using a conductivity meter.

2.2.2. Groundwater and River Water Observations

Groundwater samples (well water and pore water) along the Maowei Sea in June 2014 were collected from domestic wells and mudflats near the sea. To avoid losses via atmospheric exchange, the well water samples were collected from the bottom aquifers by an organic glass hydrophore. River water was collected from the lower salinity zone of Maolingjiang River and Qinjiang River. Then, the ^{222}Rn well water and river water samples were collected into RAD-H_2O 250 mL bottles using the overflow method until they overflowed vertically to approximately half of the bottle volume; then bottles were was quickly covered with the caps. Pore water was slowly collected (approximately 0.5 L min^{-1}) in the RAD-H_2O 250 mL bottles using a push-point piezometer and a peristaltic pump (Charette & Allen, 2006). The ^{222}Rn activities of all samples were immediately analyzed using a RAD7 detector. For all groundwater and river water samples, ancillary data (salinity and temperature) were monitored using an YSI-EC300A conductivity meter, and nutrient samples were collected.

2.3. Analytical Methods

2.3.1. ^{222}Rn Analysis

We measured the ^{222}Rn samples with a RAD7 detector that used a continuous ^{222}Rn-in-air monitor adapted for ^{222}Rn-in-water measurements. The ^{222}Rn activities were determined by counting the daughters (^{218}Po) in a silicon detector. The samples were analyzed using a RAD7 detector with RAD-H_2O and RAD-AQUA accessories. The RAD-H_2O accessory can aerate ^{222}Rn samples for 5 min and deliver the gas into a detector. The counting begins automatically after another 5 min, after which balance is reached between the ^{222}Rn and ^{218}Po. The RAD-H_2O accessory was used to analyze the well water and pore water samples. One well water or pore water sample was set to 2 h, with 12 recycles of 5 min (Durridge Co., Inc.). The RAD-AQUA accessory was used for continuous measurements of ^{222}Rn in the seawater (Figure 3b). The specific operation for the RAD-AQUA accessory was described in section 2.2.1.

2.3.2. ^{226}Ra Analysis

Fifty liter water samples were filtered through cellulose acetate membranes (pore size: 0.45 μm) and then a MnO_2-impregnated acrylic fiber column (20 g) using a ~0.5 L min^{-1} flow rate to collect the dissolved ^{226}Ra. These fibers were then thoroughly washed with Milli-Q water or purified water to remove all of the salts and were taken to a laboratory for measurement (Gu et al., 2012). The fiber samples were sealed for more than 20 days to allow the ^{222}Rn and its daughters to reach secular equilibrium with ^{226}Ra; then, the ^{226}Ra activity was determined using a RAD7 detector (Kim et al., 2001; Zhang et al., 2016).

2.3.3. Nutrient Analysis

Polyethylene 250 mL bottles were used to collect water, which was then immediately filtered to approximately 60 mL with 0.45 μm cellulose acetate filters that had been cleaned with hydrochloric acid and rinsed with Milli-Q water. Then, three to four drops of saturated $HgCl_2$ were added to the sample and kept away from the light (Ji et al., 2013; Su et al., 2011; X. L. Wang et al., 2014). The nutrients were analyzed using an autoanalyzer (Model: Skalar SANplus146; Liu et al., 2005, 2009).

2.4. Sediment Equilibration Experiments

To estimate the diffusive flux of ^{222}Rn from the sediment, five sediment samples (S1–S5 shown in Figure 2) were collected from the seabed. Because the sediments gradually become coarser from the bayhead to the mouth of the Maowei Sea (Editorial Board of China Bay Survey, 1993), we collected five sediment samples from the mouth of the Maowei Sea to near the bayhead. The porosity of the seabed sediments changed from 0.21 to 0.60. The water depth of these sediment sampling stations ranged from ~2 to 5 m. Sediment equilibration experiments were performed to estimate the diffusive flux of ^{222}Rn. Each wet sediment sample (approximately 100 g) was sealed in an Erlenmeyer flask with approximately 400–500 mL of seawater for 20 days. Then, the ^{222}Rn and ^{226}Ra activities in the sediments and overlying seawater could be approximated to reach radioactive decay equilibrium. Next, the equilibrated seawater in the RAD-H_2O 250 mL bottles was immediately analyzed using a RAD7 detector. The equilibrium activity (C_{eq}) was calculated using the porosity (φ) and wet bulk density (ρ_{wet}) of the sediments (Cable et al., 1996, 2004). Then, the diffusive flux of ^{222}Rn was calculated using the following equation (Martens et al., 1980; Ullman & Aller, 1982):

$$F_{sed} = (\lambda_{Rn-222} \times \varphi \times D_m)^{0.5}(C_{eq} - C_o) \tag{2a}$$

where C_o is the ^{222}Rn activity in the overlying water. The molecular diffusion coefficient (D_m) was described by Peng et al. (1974) as follows:

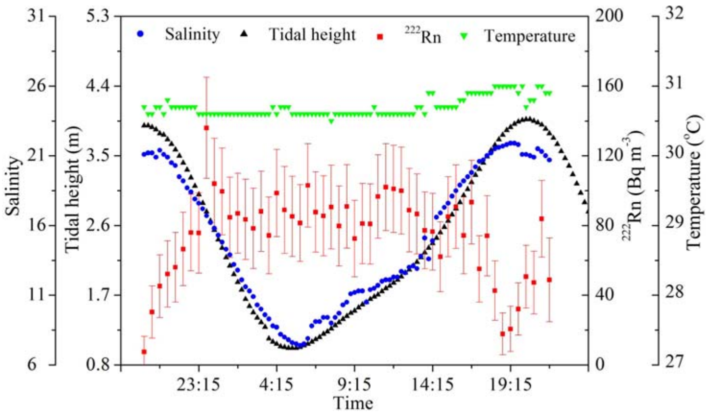

Figure 4. The variation of ^{222}Rn activities (red squares), salinity (blue dots), and temperature (green down triangles) of seawater versus tidal height (black up triangles) during the time series observation.

$$D_m = 10^{-\left(\frac{980}{T+273}+1.59\right)} \tag{2b}$$

where the T is the water temperature (°C).

3. Results

3.1. ^{222}Rn Activities and Nutrients for Time Series Observations at the TS Station

The continuous ^{222}Rn observation, as well as the salinity and temperature in the water column near the mouth of the Maowei Sea, is shown in Figure 4. The seawater temperature varied with diurnal trend dominated by solar radiation, and the temperatures were higher from noon to sunset (Figure 4). The mean temperature was 30.7°C, and a maximum diel variation of 0.5°C was observed during the time series observation. The salinity sharply dropped from 21.4 to 7.4 during the ebb tide and rose from 7.4 to 21.9 during the flood tide. As was expected, the ^{222}Rn activity was higher during the ebb tide, with a range from 7.52 to 136 Bq m^{-3}. The ^{222}Rn activity changed from 136 to 17.8 Bq m^{-3} during the flood tide. The nutrients (DIN, DIP, and DSi) exhibited similar trends as ^{222}Rn, with the DIN, DIP, and DSi concentrations (μmol L^{-1}) dropping from 64.8, 1.50, and 105 at low tide to 33.0, 0.52, and 22.0 at high tide, respectively (Figure 5). Many studies have used the tidal period cyclicity of the ^{222}Rn in seawater to reflect the dilution of offshore waters at flood tide, offshore mixing, and SGD variations (Burnett & Dulaiova, 2003; Kim & Hwang, 2002; Lambert & Burnett, 2003; Tse & Jiao, 2008). Due to tidal pumping, the recirculated seawater drains out during ebb tides and seeps into the seabed sediments during flood tides. Simultaneously, the hydrostatic pressure is lowered and the hydraulic gradient between seawater and groundwater increases, which leads to a large SGD flux at low tide. Contrarily, it contributes to a smaller SGD or even recharge of groundwater flux at high tide.

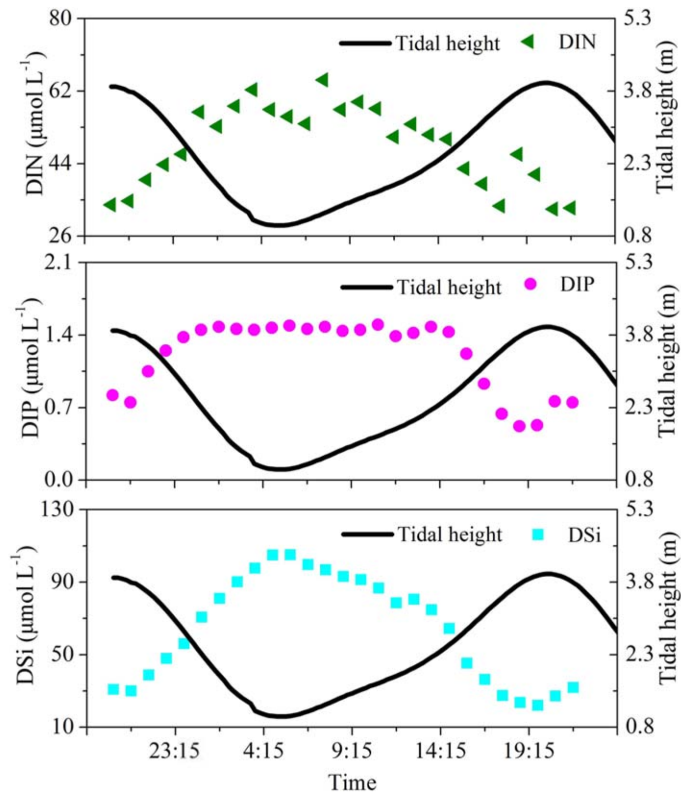

Figure 5. Temporal variation of nutrient concentrations (DIN, DIP, and DSi) as well as tidal height during the time series observation.

3.2. ^{222}Rn and Nutrients in the Groundwater and River Water

The groundwater properties (well water and pore water) along the coastal zones of the Maowei Sea are shown in Table 1. The temperature (°C) and salinity of the groundwater ranged from 24.5 to 28.8 and 0 to 20.1, respectively. The ^{222}Rn activities (Bq m^{-3}) of the groundwater changed from 1.79×10^3 to 3.81×10^4. The DIN (μmol L^{-1}), DIP (μmol L^{-1}), and DSi (μmol L^{-1}) of the groundwater varied from 2.8 to 1.04×10^3, 0 to 26.0 and 1.09×10^2 to 6.72×10^2, respectively. Obviously, the ^{222}Rn activities and nutrient concentrations in the groundwater were much higher than those in the seawater, which suggests that groundwater discharge is an important source of ^{222}Rn and nutrients in the Maowei Sea. The ^{222}Rn activities (Bq m^{-3}) of the Maolingjiang River and Qinjiang River were 234 and 160–250, respectively. The DIN (μmol L^{-1}), DIP (μmol L^{-1}), and DSi (μmol L^{-1}) were 62.4, 1.81, and 128 for the Maolingjiang River, and 101–131, 1.48–7.13, and 134 for the Qinjiang River, respectively.

4. Discussion

4.1. The Mass Balance of ^{222}Rn in the Maowei Sea

To determine the ^{222}Rn flux that was contributed from SGD, the fluxes of all ^{222}Rn sources and sinks should first be estimated. The ^{222}Rn sources include SGD input (F_{SGD}), influx during flood tides (F_{in}), ingrowth rate of dissolved ^{226}Ra in the water column ($F_{Ra\text{-}226}$), and diffusion flux from surface sediment into the water column (F_{sed}). The ^{222}Rn sinks include outflux during ebb tide (F_{out}), atmospheric

Table 1
The Temperature, Salinity, Water Depth, ^{222}Rn Activities, and Nutrient Concentrations (DIN, DIP, and DSi) of the Groundwater (Well Water and Pore Water) Collected Along the Coastal Zones of the Maowei Sea in June 2016

Station	Longitude (°E)	Latitude (°N)	Temperature (°C)	Salinity	Depth[a] (m)	Distance from sea (m)	^{222}Rn (Bq m^{-3})	Error	DIN (μmol L^{-1})	DIP (μmol L^{-1})	DSi (μmol L^{-1})	N/P ratio
G[b]1	108.5928	21.8524	26.1	0.6	38	nd	38,100	1,400	201	3.07	672	66
G2	108.5786	21.7942	27.7	0.1	4	300	2,070	400	192	0.01	143	17,000
G3	108.4763	21.8323	25.2	0.1	nd[c]	25	3,070	400	156	0	146	nd
G4	108.4972	21.8129	25.5	0	2	150	9,670	470	24.3	0.01	143	2,600
G5	108.4976	21.8136	26.6	0.1	100	100	4,770	480	12.7	0.27	165	48
G6	108.5415	21.7388	26.2	0.3	3.2	nd	6,020	460	1040	26.0	213	40
G7	108.6134	21.8224	25.2	0	1.6	nd	5,010	500	53.5	0.62	115	86
G8	108.5813	21.7763	24.5	0.5	4	250	18,700	900	866	10.6	582	81
G9	108.6053	21.7153	24.5	0.2	>6	600	7,560	600	508	0.27	122	1,900
G10	108.6251	21.7278	25.7	0.2	3.4	800	3,550	400	140	16.2	171	9
G11	108.5445	21.9099	24.5	0.3	6.5	200	1,790	370	262	4.78	281	55
G12	108.4867	21.8244	25.9	0.3	4.5	300	2,310	410	421	0.94	152	446
G13	108.4961	21.8085	28.8	0.1	1.7	600	2,830	390	2.8	0.01	126	284
G14	108.5115	21.7777	27.1	0.1	3	200	2,160	390	38.3	0.04	115	8,674
G15	108.5150	21.7768	24.7	0.2	38	100	5,980	590	83.9	0.02	163	4,910
G16	108.5484	21.7428	25	0	2	180	11,500	800	55.4	0.02	109	2,530
P[d]1	108.5943	21.7452	nd	17.6	0.7	0	4,340	510	70.8	1.55	195	46
P2	108.5980	21.7393	nd	20.1	0.6	0	1,930	200	47.6	2.01	242	24
P3	108.6046	21.8638	nd	8.8	nd	0	6,310	370	83.2	0.19	309	433

[a]Well water depth (well water samples) or the depth below the sediment-water interface (pore water samples). [b]Well water. [c]Not determined. [d]Pore water.

evasion (F_{atm}), decay loss of ^{222}Rn (F_{dec}), and mixing loss of ^{222}Rn with offshore waters (F_{mix}) in the coastal zone.

A ^{222}Rn mass balance model, which was improved from Burnett and Dulaiova (2003), was used to estimate the SGD. Based on this model, we obtained the ^{222}Rn flux from SGD by calculating the fluxes of all ^{222}Rn sources and sinks (Figure 1) in the Maowei Sea. The equation for the ^{222}Rn mass balance model can be written as follows (Zhang et al., 2016):

$$F_{SGD}+F_{riv}+F_{in}+F_{Ra-226}+F_{sed}-F_{out}-F_{atm}-F_{dec}-F_{mix}=\Delta F \tag{3}$$

where ΔF is the difference in the flux of the ^{222}Rn inventory between two successive hours, and all of the flux units for the sources and sinks are Bq m^{-2} h^{-1}.

After being corrected for other sources and sinks, the ^{222}Rn flux attributed to SGD was obtained. Using the ^{222}Rn activity in the groundwater end-member entering the system (C_{gw}, Bq m^{-3}) and SGD flux (F_{SGD}, Bq m^{-2} d^{-1}), the SGD rate (v, m d^{-1}) could be converted using the following equation:

$$v=\frac{F_{SGD}}{C_{gw}} \tag{4}$$

4.1.1. The Major Inputs of ^{222}Rn Into the Maowei Sea

For this study, the ^{222}Rn from river input (F_{riv}) is also an integral part of ^{222}Rn in the Maowei Sea and is estimated by multiplying the river discharge by the ^{222}Rn activity in the river water. Here the river discharge rates from the Maolingjiang River (http://www.zwbk.org/MyLemmaShow.aspx?lid=469852) and the Qinjiang River (http://www.zwbk.org/MyLemmaShow.aspx?lid=465957) are 127 and 107 m^3 s^{-1}, respectively. Thus, the F_{riv} was calculated to be (1.86 ± 0.34) × 10^8 Bq h^{-1} (i.e., 1.38 ± 0.25 Bq m^{-2} h^{-1}).

The effects of the tide on the change of ^{222}Rn activity cannot be ignored in the surface seawater. Therefore, it is necessary to normalize the ^{222}Rn activity to a mean tide level to eliminate the effects of tide level variations on radon when estimating the SGD (Tse & Jiao, 2008; Wen et al., 2014). The ^{222}Rn is removed from the bay with the outgoing waters at ebb tide, whereas extra ^{222}Rn is added to the bay with incoming waters during flood tide. The input fluxes of ^{222}Rn (F_{in}) with incoming water and the output fluxes of ^{222}Rn (F_{out}) with outgoing water were determined using the following equations (Zhang et al., 2016):

$$F_{in} = \frac{h_{t+\Delta t} - h_t}{\Delta t}\left(b\overline{C_w} + (1 - b)C_{off}\right) \tag{5a}$$

$$F_{out} = \frac{h_t - h_{t+\Delta t}}{\Delta t}C_w \tag{5b}$$

where h_t and $h_{t+\Delta t}$ are the water depth at time t and (t + Δt), respectively; Δt is the time interval (1 h in this study); $\overline{C_w}$ is the mean activity of ^{222}Rn in the seawater column; and C_{off} is the mean activity of ^{222}Rn in offshore water. C_w is the seawater activity of ^{222}Rn over a time interval at a time series station; b is the return flow factor (the portion of the water that leaves the estuary during ebb tide and returns unmixed during the next flood tide). Thus, we used a 3-end-member mixing model to estimate the return flow factor (Kim et al., 2008; Moore, 2003; Moore et al., 2006):

$$f_S + f_R + f_G = 1 \tag{5c}$$

$$S_S f_S + S_R f_R + S_G f_G = S_M \tag{5d}$$

$$DSi_S f_S + DSi_R f_R + DSi_G f_G = DSi_M \tag{5e}$$

where f_x (x = S, R, and G) is the fraction of seawater (S), river water (R) and groundwater (G) end-members; S_x and DSi_i are the salinity and DSi concentrations in each end-member; and S_M and DSi_M are the salinity and DSi concentrations in the surface water samples. These equations can be solved for the fractions of each end-member in each system. The 3-end-member mixing model estimates the amount of seawater in the study area, which is simply the return flow (Moore et al., 2006). The f_S, f_R, and f_G were 0.58, 0.07, and 0.35, respectively. Thus, we estimated that the return flow factor (b = f_S) was 0.58 in the Maowei Sea. Based on equation (5a), the F_{in} ranged from 0.46 to 15.8 Bq m^{-2} h^{-1} during the time series observation.

The dissolved ^{226}Ra activity in the seawater ($C_{Ra\text{-}226}$) ranged from 2.01 to 4.86 Bq m^3 with a mean of 3.17 Bq m^3 at the time series station. The supported flux in ^{222}Rn from the dissolved ^{226}Ra is as follows:

$$F_{Ra-226} = \lambda_{Rn-222} \times C_{Ra-226} \times h \tag{6}$$

where $\lambda_{Rn\text{-}222}$ is the decay constant of ^{222}Rn (0.181 day^{-1}). The $F_{Ra\text{-}226}$ ranged from 0.09 to 0.16 Bq m^{-2} h^{-1} during the time series observations.

The ^{222}Rn diffusive flux from seabed sediments was estimated using equation (2a). According to the sediment equilibration experiments, the mean porosity of the seabed sediments is 0.35, and the mean activity of ^{222}Rn in the pore water is estimated to be 7600 ± 4060 Bq m^{-3}. Thus, the ^{222}Rn diffusive flux from the seabed sediments ranged from 0.90 to 0.91 Bq m^{-2} h^{-1}.

Furthermore, as a very important source, the ^{222}Rn fluxes from SGD are calculated in section 4.2 based on the ^{222}Rn mass balance model.

4.1.2. The Major Outputs of ^{222}Rn From the Maowei Sea

The variations in the inventory of ^{222}Rn (ΔF) in the seawater over each time interval (Δt) were calculated with the following equation (Zhang et al., 2016):

$$\Delta F = \frac{I_{t+\Delta t} - I_t}{\Delta t} \tag{7}$$

where I is defined as the product of ^{222}Rn activity in the water (C_w, Bq m^{-3}) and the water depth (h, m). Thus, we determined that the ΔF ranged from −232 to 203 Bq m^{-2} h^{-1} during the time series observations. The positive values indicate an increase in ^{222}Rn inventory during the time series observation, whereas the negative values reflect a decreasing ^{222}Rn inventory.

Based on equation (5b), the F_{out} ranged from 4.9 to 52.8 Bq m^{-2} h^{-1} during the time series observation.

As a slightly soluble gas in water, ^{222}Rn always exchanges across the air-water interface when the ^{222}Rn in the two phases is in equilibrium, as follows:

$$C_w = \alpha C_{air} \tag{8a}$$

where C_{air} is the activity of ^{222}Rn in the air (Bq m^{-3}); α is the partition coefficient, and C_w is the seawater activity of ^{222}Rn, which were mentioned in equations (1) and (5b), respectively. When $C_w > \alpha C_{air}$, the diffusive flux of ^{222}Rn from the water to the air is more than the diffusive flux of ^{222}Rn from the air to the water. Then, the seawater ^{222}Rn will escape to the atmosphere, and the atmospheric evasion flux can be calculated as follows (MacIntyre et al., 1995):

$$F_{atm} = k(C_w - \alpha C_{air}) \tag{8b}$$

where k is the gas transfer velocity. The gas transfer velocity can be determined with an experimental equation, as follows (Lambert & Burnett, 2003; MacIntyre et al., 1995):

$$k_{600} = \begin{cases} 0.45u^{1.6}\left(\dfrac{S_c}{600}\right)^{-0.5} (u > 3.6\ \mathrm{m\ s^{-1}}) \\ 0.45u^{1.6}\left(\dfrac{S_c}{600}\right)^{-0.6667} (u \leq 3.6\ \mathrm{m\ s^{-1}}) \end{cases} \tag{8c}$$

where k_{600} is the gas transfer velocity normalized to the Schmidt number of CO_2 at 20°C in freshwater (cm h^{-1}); u is the wind speed (m s^{-1}); S_c (Schmidt number) is the ratio of the kinematic viscosity to the molecular diffusion coefficient (Pilson, 1998); and the kinematic viscosity is the ratio of the absolute viscosity to the density of the water (Zhang et al., 2016).

During the monitoring periods, the wind speed changed from 2.5 and 5.8 m s^{-1}. Based on the above equations, the atmospheric evasion flux for ^{222}Rn ranged from 0.68 to 8.07 Bq m^{-2} h^{-1}.

Based on the decay equation, the flux of decay loss for ^{222}Rn (F_{dec}) was calculated by the following equation:

$$F_{dec} = \lambda_{Rn-222} \times \left[C_w \times \left(1 - e^{-\lambda_{Rn-222}\Delta t}\right)\right] \times h \tag{9}$$

From this equation, we obtained that the F_{dec} ranged from 6.9×10^{-3} to 3.6×10^{-2} Bq m^{-2} h^{-1}.

The net ^{222}Rn flux (F_{net}) represents the observed fluxes of ^{222}Rn into the coastal water column with all necessary corrections (such as tidal effects, ^{226}Ra support, decay loss of ^{222}Rn, sediment diffusion, and atmospheric evasion) except for losses via mixing with lower activity waters offshore. Figure 6 shows the temporal variations of the net flux of ^{222}Rn with a histogram after correction, where the cyan line represents the mixing loss. Therefore, the net ^{222}Rn flux is described as (Zhang et al., 2016):

$$F_{net} = \Delta F - F_{riv} - F_{in} - F_{Ra-226} - F_{sed} + F_{out} + F_{atm} + F_{dec} \tag{10}$$

The net ^{222}Rn fluxes should maintain a balance between the SGD supply and mixing loss, and the fluxes ranged from −246 to 258 Bq m^{-2} h^{-1} during the time series observation. Since the conservative estimates of the mixing loss provide estimations of the minimum SGD flux, we selected the maximum negative net ^{222}Rn fluxes (–246 to −1.75 Bq m^{-2} h^{-1}) as the mixing loss fluxes. The mixing losses ranged from 1.75 to 246 Bq m^{-2} h^{-1} during the time series observation.

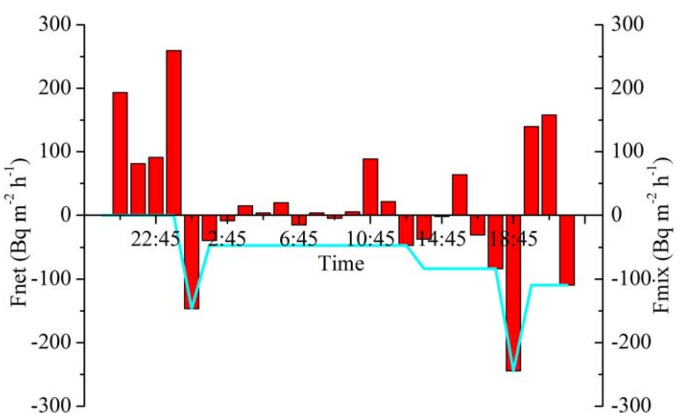

Figure 6. Net ^{222}Rn flux (rectangles) and mixing loss of ^{222}Rn (cyan line) versus time based on continuous ^{222}Rn observation at the TS station.

4.2. SGD and Its Derived Nutrient Fluxes Into the Maowei Sea

4.2.1. SGD Into the Maowei Sea

According to the ^{222}Rn mass balance model, the net ^{222}Rn flux is a balance between SGD and mixing loss into the open sea. Thus, SGD-derived ^{222}Rn fluxes (F_{SGD}) were obtained as follows:

$$F_{SGD} = F_{net} + F_{mix} \tag{11}$$

As mentioned in section 4.1, we selected the maximum negative net ^{222}Rn fluxes as the mixing loss fluxes. Therefore, the SGD-derived ^{222}Rn fluxes ranged from 0 to 260 Bq m^{-2} h^{-1} during the time series observation. Here the zero fluxes are the results of using the maximum negative net ^{222}Rn fluxes as a conservative estimate of mixing loss.

The mass balance of ^{222}Rn in the Maowei Sea is shown in Figure 7. In terms of the ^{222}Rn sources, the SGD input, influx during flood tides, river input, sediment diffusion, and ingrowth of dissolved ^{226}Ra accounted for 86%, 11%, 2%, 1%, and 0.1% of the ^{222}Rn sources,

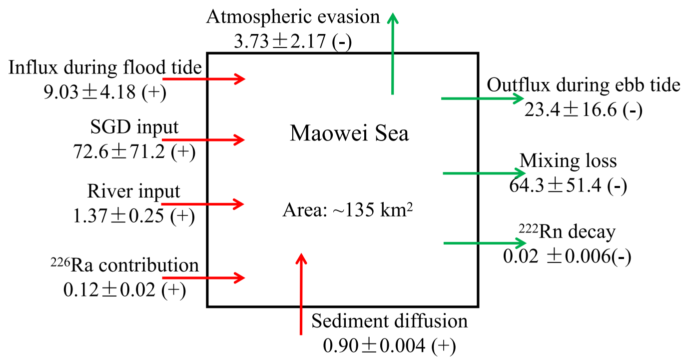

Figure 7. The ^{222}Rn sources (+) and sinks (–) (all in Bq m^{-2} h^{-1}) during June 2016 in the Maowei Sea (here the SGD input is a conservative estimate and the others are mean values).

respectively. The ^{222}Rn sinks, including the mixing loss with offshore waters, outflux during ebb tide, atmospheric evasion, and decay loss of ^{222}Rn accounted for 70%, 26%, 4%, and 0.02% of the ^{222}Rn sinks, respectively.

The SGD-derived ^{222}Rn fluxes were estimated by multiplying the SGD rate by the ^{222}Rn activity in the groundwater end-members. Commonly, the selection of an appropriate end-member is the main source of uncertainty in SGD estimates (Burnett et al., 2008; Cerdà-Domènech et al., 2017; Cho & Kim, 2016). Thus, the option of groundwater end-members is very important for estimating the SGD-derived nutrients. In the present study, the ^{222}Rn activities in the well water varied widely, ranging from 1,790 to 38,100 Bq m^{-3}, and the ^{222}Rn activities in the pore water ranged from 1,930 to 6,310 Bq m^{-3}. The large variability of the ^{222}Rn activity in the groundwater along the coast of the Maowei Sea is likely associated with the distance from the coastal line, sampling depth, heterogenic geological matrix, and highly dynamic aquifer system. Generally, many previous studies selected the well water or pore water near the shore as the groundwater end-members (e.g., Hwang et al., 2016; Peterson et al., 2009; Santos et al., 2011; Wang et al., 2017). Here we selected the well water samples that were collected from the shallow water wells closest to the coastal line (the maximum distance from the coastal line is approximately 200 m) and the pore water samples as the groundwater end-members (such as G3, G4, G11, G14, G16, P1, P2, and P3). If it is assumed that these stations represent the ^{222}Rn activity in groundwater in only the point-source of groundwater discharge (Peterson et al., 2009), the mean ^{222}Rn activity in the groundwater end-members can be estimated to be 5,100 $\pm$ 3,490 Bq m^{-3}. Based on equation (4), the SGD rate in the Maowei Sea was calculated to be 0–1.22 m d^{-1} with a mean of 0.36 $\pm$ 0.33 m d^{-1}. Thus, the SGD flux in the Maowei Sea was 4.9 $\times$ 10^7 m^3 d^{-1}. The SGD is the mixture of terrestrial fresh groundwater and recirculated seawater and is not only freshwater discharge. In many cases, the percentage of recirculated seawater is greater than 85% (e.g., Liu et al., 2017; Santos et al., 2009; Taniguchi et al., 2005; X. Wang et al., 2015).

The total SGD flux in each specific subterranean estuary is driven by different forces (e.g., tides, waves, freshwater gradients, density gradients, and seasons; Michael et al., 2011). Table 2 summarizes the typical SGD fluxes into bays in different regions around the world, which shows that the SGD rate in the Maowei Sea is within the range of SGD rates in bay systems around the world. The SGD fluxes in these bay systems may be influenced by precipitation, tidal range, etc. The input of rainwater into the highly permeable aquifers could increase the discharge of terrestrial fresh groundwater into coastal bay systems. During this process, terrestrial hydraulic gradients play important roles in the discharge of terrestrial fresh groundwater (Wang & Du, 2016). Because SGD includes both terrestrial fresh groundwater and recirculated seawater, the increase in local precipitation will increase the SGD flux in each subterranean estuary. For example, the tidal ranges of the bays along the Chinese coasts are approximately the same and vary from 0.9 to 1.1 m (Table 2; i.e., G. Wang et al., 2014; Tse & Jiao, 2008; Wang et al., 2017; X. L. Wang et al., 2014; Zhang et al., 2016). We found that the SGD rates are positively correlated with the local precipitation in these bay systems ($r = 0.58$, $p > 0.05$). It appears that precipitation may affect the SGD in some subterranean estuaries. For example, the SGD flux in the Jiulong River estuary (China) in the summer (rainy season) was significantly higher than that in other seasons, which indicates that the SGD flux rapidly responds to precipitation (G. Z. Wang et al., 2015). The impacts of tidal ranges and aquifer recharge on the hydraulic gradient have been extensively reported (e.g., Bokuniewicz et al., 2008; Gonneea et al., 2013; Michael et al., 2011; Moore & Wilson, 2005). The SGD rates were found to be higher at low tides than high tides in many bays (e.g., Bokuniewicz et al., 2008; Tse & Jiao, 2008; Wang & Du, 2016; Zhang et al., 2016). However, the interaction between SGD and tides was nonlinear, indicating that a higher tidal range could drive the recirculation of seawater into the coastal sediments at much wider temporal and spatial scales. This physical process could also cause a hydraulic gradient that could drive coastal pore water (including recirculated seawater and terrestrial fresh groundwater) into the seawater of the bay systems (Bokuniewicz et al., 2008). As a physical force, the tidal range is relevant to the determination of freshwater-seawater mixing in most coastal areas. However, the tidal influences are diverse in different coastal aquifer systems (Cerdà-Domènech et al., 2017; Charette,

Table 2
A Comparison of the SGD Rates, the Local Precipitation, and Tidal Ranges for Bay Systems Worldwide

Study area		SGD rate ($cm\ d^{-1}$)	Precipitation ($mm\ yr^{-1}$)	Tidal range (m)	Reference
North America					
Indian River Lagoon, FL, USA		1–12	1,110–1,300	0.02–0.05	Cable et al. (2006)
Florida Coastal Lagoon, USA		3–20	1,230–1,340	0.1	Cable et al. (2004)
Waquoit Bay, USA		2.3	1,260[a]	1.1	Michael et al. (2011); Gonneea et al. (2013)[a]
South America					
Patos Lagoon, Brazil		0.54		0.5	Niencheski et al. (2007)
Patos Lagoon coastal zone, Brazil		0.54–2.2		0.5[b]	King (2012); Niencheski et al. (2007)[b]
Mangueira Lagoon, southern Brazil		25	696		Santos et al. (2008)
Flamengo Bay, Brazil		5–400	1,200	0.7–1.2	Bokuniewicz et al. (2008)
Europe					
Marn Menor, Spain		0.08–3.86	300	0.02–0.03	Baudron et al. (2015)
Lesina Lagoon, Italy		1.76	840	0.05	Rapaglia et al. (2012)
Venice Lagoon, Italy		2.8–16.6	332.7	1	Ferrarin et al. (2008)
		6.0–8.2		0.3–1.2	Rapaglia et al. (2010)
North Venice, Italy		0.71–4.29	766.4	0.65	Garcia-Solsona et al. (2008)
Southern Venice, Italy		0.75–2.45	532.4	0.8	Gattacceca et al. (2011)
Bay of Puck, Southern Baltic Sea		0.3–2.2	560		Szymczycha et al. (2012)
Oceania					
Queensland, Australia	Welsby	3.4	1,420	1.3[b]	Sadat-Noori et al. (2016); Knight et al. (2008)[b]
	South Welsby	7.3	1,420	1.3[b]	
	Mermaid	2.6	1,420	1.3[b]	
North Creek, Australia		48.9–64.5	1,800		Atkins et al. (2013)
Rarotonga, Australia		16.7	2,100	0.56	Cyronak et al. (2014)
Heron Island, Australia		29.7	1,028	2.1	
Korogoro creek, Australia		24–68	1,490		Sadat-Noori et al. (2015)
Asia					
Eastern Laizhou Bay, China		6.93	630	0.9	Zhang et al. (2016)
Sanggou Bay, China		1–14	816.24[a]	1.1	X. L. Wang et al. (2014); [a]Wang (2017)
Sanya Bay, China		25–44	1,417	0.94	G. Wang et al. (2014)
Daya Bay, China		28.2–30.9	1,700	0.9	Wang et al. (2017)
Tolo Harbour, Hong Kong		7.8–63	2,214	0.97	Tse and Jiao (2008)
Xiangshan Bay, China		23–69	1,500	3.18	Wu et al. (2013)
Bangdu Bay, Korea		33–49	1,900		Hwang et al. (2005)
Western India		5–280	3,000		Rahaman and Singh (2012)
Maowei Sea		36 ± 33	2,140	2.5	This study

[a]The references supply only precipitation in the relevant study areas. [b]The references supply only the tidal range in the relevant study areas.

2007; Kim & Hwang, 2002; Michael et al., 2003); they play minor roles in microtidal environments such as the Mediterranean Sea (Cerdà-Domènech et al., 2017; Garcia-Solsona et al., 2010), the Baltic Sea (Szymczycha et al., 2012), and the Caribbean Sea (Gonneea et al., 2014). However, these microtidal coastal aquifers are highly influenced by precipitation (Cerdà-Domènech et al., 2017). Because the Maowei Sea is characterized by a larger tidal range (2.5 m) and higher precipitation (2,140 mm; Tian et al., 2014), the SGD flux in the Maowei Sea may be mainly controlled both by the tide and precipitation. Many other factors (e.g., seasonal sea level changes (Moore, 2010), seabed topography (Konikow et al., 2013), and water-sediment regulation (Xia et al., 2016)) could also influence the SGD, and they deserve further study.

4.2.2. Groundwater-Borne Nutrients in the Maowei Sea

The groundwater-borne nutrient fluxes into the bay were estimated by multiplying the SGD rates by the nutrient concentrations in the groundwater end-members. In this study, the concentrations of DIN, DIP, and DSi ($\mu mol\ L^{-1}$) in the groundwater (well water and pore water) had wide ranges of 2.8–1,040, 0–26, and 109–672 ($n = 19$), respectively. The nutrient concentrations in groundwater are variable and depend on the soil and aquifer characteristics, aquifer permeability, groundwater recharge rate and climate (Slomp & Van Cappellen, 2004). In addition, anthropogenic activities (e.g., fertilizer use and sewage discharge) are also one of the most important sources of nutrients in groundwater. To avoid overestimating the nutrient fluxes from SGD, we selected the well water samples that were collected from the shallow water wells closest to the coastal line (the maximum distance from the coastal line was approximately 200 m) and the pore water samples as the groundwater end-members of the nutrients (such as G3, G4, G11, G14, G16, P1, P2, and P3), which were 24.3–262, 0–4.78, and 109–309 μmol L^{-1} for DIN, DIP, and DSi, respectively. In the present study, the TS station is close to the open sea, and the SGD rate is commonly smaller at TS station. If the SGD rate at the TS station is assumed to be conservative and representative of the entire Maowei Sea, the SGD-derived nutrient fluxes (mol d^{-1}) into the Maowei Sea would be equivalent to (1.2–13) $\times$ 10^6 (mean: (4.5 $\pm$ 5.5) $\times$ 10^6), (0–2.3) $\times$ 10^5 (mean: (5.3 $\pm$ 9.1) $\times$ 10^4), and (5.3–15) $\times$ 10^6 (mean: (9.4 $\pm$ 9.3) $\times$ 10^6) for DIN, DIP, and DSi, respectively.

The river nutrient fluxes were estimated by multiplying the river discharge by the nutrient concentrations in the river water. The DIN, DIP, and DSi input fluxes (mol d^{-1}) from the rivers around the coast of the Maowei Sea were (2.3 $\pm$ 0.7) $\times$ 10^6, (6.0 $\pm$ 5.1) $\times$ 10^4, and (2.6 $\pm$ 0.1) $\times$ 10^6, respectively. The SGD-derived nutrients (i.e., DIN, DIP and DSi) were at least 1.9, 0.9, and 3.6 times the local river input in June in the Maowei Sea. In many cases, the fluxes of SGD-derived nutrients are also larger than the fluxes from the local rivers, as was observed in Sanggou Bay, China (X. L. Wang et al., 2014), Eastern Laizhou Bay, China (Zhang et al., 2016), and Maalaea and Kuau, USA (Bishop et al., 2015). The nutrient fluxes from atmospheric wet deposition (mol d^{-1}) were estimated by $C_{rain}PS$, where C_{rain}, P and S were the nutrient concentrations of rainwater, the monthly rainfall (the rainfall was 385.1 mm in June 2016 in the Maowei Sea; http://www.gxwater.gov.cn/Web/report/YL_LntqCompare.aspx) and the area of the Maowei Sea, respectively. Therefore, the nutrient fluxes from atmospheric wet deposition (mol d^{-1}) were (10 $\pm$ 5) $\times$ 10^4, (3.7 $\pm$ 3.7) $\times$ 10^2, and (3.6 $\pm$ 1.1) $\times$ 10^3 for DIN, DIP, and DSi, respectively. Here the nutrient fluxes from atmospheric dry deposition (mol d^{-1}) were the mean values along the coast of China (Bi, 2006; Chen et al., 2010; Han, 2013; Zhu, 2011; Zou et al., 2011), which were (3.0 $\pm$ 1.2) $\times$ 10^4, (2.4 $\pm$ 2.8) $\times$ 10^2, and (7.4 $\pm$ 2.8) $\times$ 10^2 for DIN, DIP, and DSi, respectively. Compared to the atmospheric deposition, the nutrient fluxes from SGD were 2–3 orders of magnitude higher than those from atmospheric deposition. It is obvious that SGD-derived nutrients are an important pathway for nutrients into estuaries and along coastlines.

4.3. Nutrient Budgets in the Maowei Sea

The Maowei Sea is the largest oyster growing area with the largest mangrove forest of China (Wu et al., 2014). Approximately 1.84 $\times$ 10^8 kg yr^{-1} of oysters are produced in the Maowei Sea (statistical data from the Fisheries Technology Extension Station in Qinzhou City: Web Interface, http://qinzhou0675.11467.com/). The inputs of DIN and DIP include SGD input, river inputs, atmospheric deposition, sewage outfalls, sediment diffusion and aquaculture. The removals of DIN and DIP include mixing losses, aquaculture harvests, organic debris deposition, and mangrove absorption and primary productivity.

4.3.1. DIN and DIP Sources in the Maowei Sea

The DIN and DIP fluxes in the Maowei Sea from SGD, rivers and atmospheric deposition in June 2016 are shown in Table 3. The DIN and DIP fluxes from sewage outfalls into the Maowei Sea were reported to be 3.9 $\times$ 10^7 and 2.8 $\times$ 10^6 mol $month^{-1}$, respectively (statistical data from the Guangxi Marine Environmental Monitoring Center: Web Interface, http://www.beihai.gov.cn/3650/intro.htm). The DIN and DIP fluxes from aquaculture wastewater into the Maowei Sea were reported to be 3.1 $\times$ 10^6 and 2.2 $\times$ 10^5 mol $month^{-1}$, respectively (Long et al., 2012). The DIN flux (DIN_{SED}) and DIP flux (DIP_{SED}) from sediment diffusion can be estimated using the following equation (Wu, 2005):

$$DIN_{SED} = R_{SED\_DIN} \times \exp(K_{SED\_DIN} \times T) \times S \tag{12a}$$

$$DIP_{SED} = R_{SED\_DIP} \times \exp(K_{SED\_DIP} \times T) \times S \tag{12b}$$

where R_{SED_DIN} (41.1 mmol m^{-2} $month^{-1}$) and R_{SED_DIP} (0.6 mmol m^{-2} $month^{-1}$) are the diffusion rates from the sediment for DIN and DIP, respectively. K_{SED_DIN} (0.04°C^{-1}) and K_{SED_DIP} (0.04°C^{-1}) are the temperature coefficients. T (°C) and S (m^2) are the temperature and area of the Maowei Sea, respectively. The DIN and DIP fluxes from the sediments were 1.9 $\times$ 10^7 and 2.8 $\times$ 10^5 mol $month^{-1}$, respectively.

4.3.2. DIN and DIP Sinks in the Maowei Sea

The Maowei Sea has a mangrove area of 23 km^2 (Zhao, 2011). According to the mean monthly absorption of DIN and DIP per square meter of mangrove (Lin, 1989), the absorptions of DIN and DIP by mangroves were 2.9 $\times$ 10^6 and 1.4 $\times$ 10^5 mol $month^{-1}$ in the Maowei Sea, respectively, and these values were based

Table 3
The DIN and DIP Budgets During June 2016 in the Maowei Sea

Sources and sinks	DIN flux (mol month^{-1})	Percentage to total DIN sources/sinks (%)	DIP flux (mol month^{-1})	Percentage to total DIP sources/sinks (%)
Sources				
SGD input	1.3×10^8	50.2	1.6×10^6	23.6
River input	6.9×10^7	25.7	1.8×10^6	26.7
Sewage outfall	3.9×10^7	14.4	2.8×10^6	42.0
Diffusion from sediment	1.9×10^7	7.1	2.8×10^5	4.1
Aquaculture	3.1×10^6	1.1	2.2×10^5	3.3
Atmospheric deposition	3.9×10^6	1.5	1.8×10^4	0.3
Sinks				
Mixing loss	8.8×10^7	32.7	2.0×10^6	30.1
Absorption by primary productivity	3.4×10^7	12.8	2.1×10^6	32.0
Organic debris deposition	6.3×10^6	2.3	5.4×10^4	0.8
Mangrove absorption	2.9×10^6	1.1	1.4×10^5	2.0
Harvest from aquaculture	1.4×10^8	51.1	2.3×10^6	35.0

on the area of mangroves and the mean monthly absorption of DIN and DIP per square meter of mangrove. The primary productivity was 671.3 mg (C) m^{-2} d^{-1} in the summer in this region (Yang et al., 2015). According to the Redfield ratio (C:N:P of 106:16:1), we calculated that the absorptions of DIN and DIP by primary productivity were 3.4×10^7 and 2.1×10^6 mol month^{-1} in the Maowei Sea, respectively. The deposition rates of dissolved organic nutrients mainly depend on the abundance of phytoplankton. Although there is no report on the deposition rate of organic debris in the Maowei Sea, the abundance of phytoplankton in the summer is approximately 10^7 cells L^{-1} (Wei & He, 2008), which is the same magnitude in Sanggou Bay (Wang et al., 2008). The deposition rate of organic debris in a bay with similar aquaculture practices (Sanggou Bay) in China was 4.7×10^{-2} mol month^{-1} m^{-2} for DIN and 4.0×10^{-4} mol month^{-1} m^{-2} for DIP (X. L. Wang et al., 2014). Therefore, we used this value to calculate that the DIN and DIP fluxes from the deposition of organic debris were 6.3×10^6 and 5.4×10^4 mol month^{-1} in the Maowei Sea, respectively. Furthermore, the mixing losses of DIN (E_{DIN_OUT}) and DIP (E_{DIP_OUT}) with offshore water outside the bay can be determined using the following equations (Wu, 2005):

$$E_{DIN\_OUT} = (DIN - DIN_{OUT}) \times S \times H/T_f \tag{13a}$$

$$E_{DIP\_OUT} = (DIP - DIP_{OUT}) \times S \times H/T_f \tag{13b}$$

where DIN and DIP are the concentrations of DIN and DIP in the Maowei Sea. DIN_{OUT} and DIP_{OUT} are the concentrations of DIN and DIP in the offshore water outside the bay. H is the mean depth of the Maowei Sea. The mean flushing time, T_f, was calculated by the classical tidal prism method (Dai Dyer & Taylor, 1973; Sanford et al., 1992). Based on equations (13a) and (13b), the mixing losses of DIN and DIP were 8.8×10^7 and 2.0×10^6 mol month^{-1}, respectively.

Given the values above, the DIN and DIP budgets for the Maowei Sea can be constructed based on a box model (Gordon et al., 1996; Wang & Du, 2016), which has been widely used to construct the DIN and DIP budgets in estuarine and coastal ecosystems (Liu et al., 2009; Wang & Du, 2016; X. L. Wang et al., 2014). Assuming that the systems were in a steady state, the DIN and DIP sources and sinks were estimated. According to this box model for nutrients, the DIN and DIP fluxes from aquaculture harvest were estimated to be 1.4×10^8 and 2.3×10^6 mol month^{-1}, respectively. All of the sources and sinks of DIN and DIP in the Maowei Sea are shown in Table 3. Based on the DIN and DIP budgets in the Maowei Sea, we found that the DIN and DIP removals from aquaculture harvest accounted for 51% and 35% of the total removals in the Maowei Sea, respectively (Table 3). To avoid overestimating the DIN and DIP fluxes from aquaculture harvest, the conservative DIN and DIP fluxes from SGD were selected in this study to calculate the DIN and DIP fluxes from aquaculture harvest.

4.4. Eco-Environmental Impacts of SGD-Derived Nutrients in the Maowei Sea

Previous studies have evaluated the eutrophication in the Maowei Sea, and the origins of the eutrophication processes were attributed to the nutrient inputs from rivers (Lan & Peng, 2011; Yang et al., 2012).

Table 4
SGD Rates and SGD-Derived Nutrient Fluxes From Previous Studies for Bay Systems Worldwide

Study area	Tracer	SGD rate (10^{-2} m d^{-1})	DIN flux (10^{-3} mol m^{-2} d^{-1})	DIP flux (10^{-5} mol m^{-2} d^{-1})	DSi flux (10^{-4} mol m^{-2} d^{-1})	References
Bangdu Bay, Korea	^{222}Rn and ^{224,226}Ra	33–49	21	16	460	Hwang et al. (2005)
Tampa Bay, USA	^{222}Rn and ^{223,224,226,228}Ra	***0.22–1.5***[a]	0.13–0.87	1.9–14	8.7–60	Swarzenski et al. (2007)
Tolo Harbour, Hong Kong	^{222}Rn	7.8–63	12–25	27–55	18–37	Tse and Jiao (2008)
Concepcion Bay, Mexico	^{222}Rn	0.4–43.9	1.6	na[b]	na	Santos et al. (2011)
Jiaozhou Bay, China	^{222}Rn	6.38–8.29	***0.128–0.132***	16	***0.42–0.47***	Guo et al. (2013)
Xiangshan Bay, China	^{222}Rn	***23–69***	***230–680***	***120–360***	32	Wu et al. (2013)
Sarasota Bay, USA	^{222}Rn	0.7–24	2.1–8.3	40–250	na	Mwashote et al. (2013)
Sanggou Bay, China	^{223,224,226,228}Ra	13–14	18–21	6.3–7.5	9.6–11	X. L. Wang et al. (2014)
Jiulong River Estuary, China	^{226}Ra	3.7–20	12–68	***0.63–3.4***	200–1,100	G. Z. Wang et al. (2015)
Obama Bay, Japan	^{222}Rn	0.61	0.54	2.1	5.6	Sugimoto et al. (2016)
Laoye Lagoon, China	^{223,224,226,228}Ra	9.4	3.3	89	***14,000***	Wang and Du (2016)
Xiaohai Lagoon, China	^{223,224,226,228}Ra	4.1	36	190	5,800	Wang and Du (2016)
Geoje Bay, Korea	^{222}Rn	5.0	2.0	3.0	59	Hwang et al. (2016)
Eastern Laizhou Bay, China	^{222}Rn	6.93	13	na	na	Zhang et al. (2016)
La Paz Bay, Mexico	^{222}Rn	10–18	2–52	4–94	70–1,640	Urquidi-Gaume et al. (2016)
Maowei Sea, China	^{222}Rn	36 ± 33	33 ± 41	39 ± 67	695 ± 688	This study

[a]Bold and italic font represent the maximum and minimum SGD rates or nutrient fluxes, respectively. [b]Not available in the studies.

However, the results from the present work indicate that the SGD-derived nutrients (i.e., DIN, DIP, and DSi) were at least 1.9, 0.9, and 3.6 times greater than the river inputs, respectively. Table 3 indicates that the mass balance estimations suggest that SGD-derived nutrients are other dominant sources in the Maowei Sea. This result means that the nutrient contributions to water eutrophication in the Maowei Sea should be reevaluated, and the nutrients derived from the SGD should receive more attention in the Maowei Sea. In the coastal ecosystems of other bay systems worldwide (Table 4), the SGD-derived DIN, DIP and DSi fluxes ranged from (0.13 to 68) $\times$ 10^{-3}, (0.63 to 250) $\times$ 10^{-5}, and (0.42 to 13,900) $\times$ 10^{-4} mol m^{-2} d^{-1}, respectively. Compared to these regions, the SGD-derived nutrient fluxes to the Maowei Sea were (33 ± 41) $\times$ 10^{-3}, (39 ± 67) $\times$ 10^{-5}, and (695 ± 688) $\times$ 10^{-4} for DIN, DIP, and DSi, respectively, which are within the ranges of the high input levels.

Significant increases of nitrogen and phosphorus loading into the bay could result in increases in the phytoplankton biomass (Hagy et al., 2004; Harding et al., 2015) or ecosystem impairments, such as the depletion of dissolved oxygen (Hagy et al., 2004; McCoy et al., 2011), red tide outbreaks (Hu et al., 2006; Lee et al., 2010; Luo & Jiao, 2016), adverse human health conditions (Townsend et al., 2003), and eutrophication (Hwang et al., 2005) as well as impacts to global nutrient cycling (Galloway et al., 2008; Slomp & Van Cappellen, 2004). In this study, we observed that the N/P ratios in the groundwater around the Maowei Sea were high (mean: 64; Table 5). This phenomenon has also been observed in other bay systems, including ratios of 43 observed in Daya Bay (China), 78 in Hampyeong Bay (Korea), 134 in Bangdu Bay (Korea), and 191 in Xiangshan Bay (China; Hwang et al., 2005; Waska & Kim, 2011; Wang et al., 2017; Wu et al., 2013). In the Maowei Sea, the mean N/P ratios were 45 in the surface seawater and 28 in the river

Table 5
The Nutrients and N/P Ratios in Groundwater, River Water, Surface Seawater, and the Seawater Column (108°33′22″E, 21°45′18″N) at Different Depths in the Maowei Sea

Type		DIN	DIP	N/P ratio	DSi
Groundwater (n = 19)		224	3.5	64	219
River water (n = 3)		98	3.5	28	132
Seawater (surface, n = 10)		53	1.2	45	84
Seawater column (n = 1)	Water depth: 0.5 m	56	1.3	42	81
	Water depth: 4 m	52	1.4	37	60
	Water depth: 8 m	45	1.3	34	56

water (i.e., the Maolingjiang River and Qinjiang River; Table 5). In the water column, the N/P ratios were 42, 37, and 34 at the water depths of 0.5 m (surface layer), 4 m (middle layer), and 8 m (bottom layer), respectively (Table 5). Although the N/P ratios in the bottom layer were lower than those in the surface and middle layers, all N/P ratios in the seawater column were obviously higher than those in the river water. That is, the N/P ratios followed an order of groundwater > seawater > river water. This result clearly reflects that the seawater N/P ratios were the result of the mixing between riverine inputs (low N/P ratios) and SGD (high N/P ratios). Since the N/P ratio is often used to evaluate the potential limitations of primary production, high N/P ratios in the groundwater could force the primary production conditions to change from N-limitation to P-limitation; thus, affecting the ecology (Lapointe et al., 1990; Slomp & Van Cappellen, 2004; Su et al., 2011) and changing the microalgal community composition (Lee et al., 2010; Su et al., 2011) of the coastal waters. Thus, we suggest that the high nutrient levels and N/P ratios in the SGD around the Maowei Sea likely exceed the limits that would allow for environmental self-purification. This condition would strongly affect this coastal ecosystem by changing the biomass and community structure of the phytoplankton, such as by gradually intensifying eutrophication events and increasing the occurrence of red tide outbreaks.

Furthermore, the N/P ratios in oysters were reported to vary from 57 to 76, with an average of 67 (Niu, 2014), which is very close to the N/P ratios (64) in the SGD in the Maowei Sea. At the same time, the nutrient budgets in the Maowei Sea exhibited DIN and DIP removals during aquaculture harvest and these removals accounted for 51% (1.4×10^8 mol month^{-1}) and 35% (2.3×10^6 mol month^{-1}) of the total DIN and DIP removals in the Maowei Sea, respectively (Table 3). Based on the estimated DIN and DIP removals from oyster aquaculture harvest, the N/P ratio of the removal from oyster aquaculture harvest was estimated to be 61, which was within the range of the N/P ratios (57–76) in oysters. In addition, the results in the present work indicate that the SGD-derived DIN and DIP were at least 1.9 and 0.9 times the local river inputs, respectively. Thus, we inferred that the SGD-derived nutrients with high N/P ratios could support oyster aquaculture in the Maowei Sea. At the same time, the harvest of oyster aquaculture can remove a large of amount of nutrients, especially DIN. A number of studies have also suggested that SGD-derived nutrients are very important and can support the production of oyster farming (e.g., Hwang et al., 2010, 2016). These observations indicate that high-density oyster aquaculture seems to lighten the burden of water eutrophication in the Maowei Sea. Nevertheless, more intensive studies are needed to prove the direct relationship between SGD and oyster aquaculture in the future, especially for the N/P ratio of SGD and N/P ratio in oysters. Therefore, it is urgent and important to strengthen environmental protection and rationally manage aquaculture, especially for oyster growth.

5. Conclusions

The Maowei Sea is a highly productive oyster aquaculture farm that is based in the Beibu Gulf. The Maowei Sea has become one of most important economic development regions in the Beibu Gulf because of its fruitful resources and strategic location. However, the marine ecological environment in the region is deteriorating due to rapid industrialization and urbanization. In this study, the SGD and nutrient fluxes into the Maowei Sea were estimated for the first time via continuous ^{222}Rn monitoring. We can draw the following conclusions:

1. The SGD rate in the Maowei Sea was estimated to be 0.36 ± 0.33 m d^{-1} in June 2016. The estimated nutrient fluxes (mol d^{-1}) via SGD were $(1.2–13) \times 10^6$ (mean: $(4.5 \pm 5.5) \times 10^6$), $(0–2.3) \times 10^5$ (mean: $(5.3 \pm 9.1) \times 10^4$), and $(5.3–15) \times 10^6$ (mean: $(9.4 \pm 9.3) \times 10^6$) for DIN, DIP, and DSi, respectively, which were more than 1.9, 0.9, and 3.6 times the fluxes from the local river inputs.
2. The high nutrient levels and N/P ratios of SGD in the Maowei Sea likely exceeded the values that would allow for environmental self-purification, which may lead to increases in the biomass and the phytoplankton community structure. These processes could affect the biogeochemical cycles and marine ecological environment in the Maowei Sea.
3. Oyster aquaculture removes a large of amount of nutrients, especially DIN, from the Maowei Sea, and appropriate aquaculture practices can mitigate the environmental harm caused by the high N/P ratios in SGD.

Acknowledgments
We thank all the colleagues of the radioisotope group from SKLEC/ECNU and Qinzhou University for their assistance in the field. This research was supported by the Natural Science Foundation of China (grants 41576083 and 41706083), the Program of the State Key Laboratory of Estuarine and Coastal Research (SKLEC-KF201703), and the Guangxi Key Laboratory of Marine Disaster in the Beibu Gulf, Qinzhou University (2017KF03). We also thank Editor, Adina Paytan, and two anonymous reviewers for their constructive comments for improvement of the original manuscript. All the data used for this paper are available in the tables reported in the text (Tables (1–5)).

References

Atkins, M. L., Santos, I. R., Ruiz-Halpern, S., & Maher, D. T. (2013). Carbon dioxide dynamics driven by groundwater discharge in a coastal floodplain creek. *Journal of Hydrology*, *493*, 30–42. https://doi.org/10.1016/j.jhydrol.2013.04.008

Baudron, P., Cockenpot, S., Lopez-Castejon, F., Radakovitch, O., Gilabert, J., Mayer, A., et al. (2015). Combining radon, short-lived radium isotopes and hydrodynamic modeling to assess submarine groundwater discharge from an anthropized semiarid watershed to a Mediterranean lagoon (Mar Menor, SE Spain). *Journal of Hydrology*, *525*, 55–71. https://doi.org/10.1016/j.jhydrol.2015.03.015

Bi, Y. F. (2006). *Atmospheric nutrient deposition at the East China coast and its impact on marine primary production* [in Chinese with English abstract] (China master's thesis). Qingdao, Shandong, China: Ocean University of China.

Bishop, J. M., Glenn, C. R., Amato, D. W., & Dulai, H. (2015). Effect of land use and groundwater flow path on submarine groundwater discharge nutrient flux. *Journal of Hydrology: Regional Studies*, *11*, 194–218. https://doi.org/10.1016/j.ejrh.2015.10.008

Boehm, A. B., Paytan, A., Shellenbarger, G. G., & Davis, K. A. (2006). Composition and flux of groundwater from a California beach aquifer: Implications for nutrient supply to the surf zone. *Continental Shelf Research*, *26*(2), 269–282. https://doi.org/10.1016/j.csr.2005.11.008

Bokuniewicz, H., Taniguchi, M., Ishitoibi, T., Charette, M., Allen, M., & Kontar, E. A. (2008). Direct measurements of submarine groundwater discharge (SGD) over a fractured rock aquifer in Flamengo Bay Brazil. *Estuarine, Coastal and Shelf Science*, *76*(3), 466–472. https://doi.org/10.1016/j.ecss.2007.07.047

Burnett, W. C., Bokuniewicz, H., Huettel, M., Moore, W. S., & Taniguchi, M. (2003). Groundwater and pore water inputs to the coastal zone. *Biogeochemistry*, *66*(1/2), 3–33. https://doi.org/10.1023/B:BIOG.0000006066.21240.53

Burnett, W. C., Cowart, J. B., & Deetae, S. (1990). Radium in the Suwannee River and estuary. *Biogeochemistry*, *10*(3), 237–255.

Burnett, W. C., & Dulaiova, H. (2003). Estimating the dynamics of groundwater input into the coastal zone via continuous radon-222 measurements. *Journal of Environmental Radioactivity*, *69*(1), 21–35. https://doi.org/10.1016/S0265-931X(03)00084-5

Burnett, W. C., & Dulaiova, H. (2006). Radon as a tracer of submarine groundwater discharge into a boat basin in Donnalucata, Sicily. *Continental Shelf Research*, *26*(7), 862–873. https://doi.org/10.1016/j.csr.2005.12.003

Burnett, W. C., Peterson, R., Moore, W. S., & de Oliveira, J. (2008). Radon and radium isotopes as tracers of submarine groundwater discharge-results from the Ubatuba, Brazil SGD assessment intercomparison. *Estuarine, Coastal and Shelf Science*, *76*(3), 501–511. https://doi.org/10.1016/j.ecss.2007.07.027

Cable, J. E., Burnett, W. C., Chanton, J. P., & Weatherly, G. L. (1996). Estimating groundwater discharge into the northeastern Gulf of Mexico using radon-222. *Earth and Planetary Science Letters*, *144*(3–4), 591–604. https://doi.org/10.1016/S0012-821X(96)00173-2

Cable, J. E., Martin, J. B., & Jaeger, J. (2006). Exonerating Bernoulli? On evaluating the physical and biological processes affecting marine seepage meter measurements. *Limnology and Oceanography: Methods*, *4*(6), 172–183. https://doi.org/10.4319/lom.2006.4.172

Cable, J. E., Martin, J. B., Swarzenski, P. W., Lindenberg, M. K., & Steward, J. (2004). Advection within shallow pore waters of a coastal lagoon, Florida. *Ground Water*, *42*(7), 1011–1020. https://doi.org/10.1111/j.1745-6584.2004.tb02640.x

Cerdà-Domènech, M., Rodellas, V., Folch, A., & Garcia-Orellana, J. (2017). Constraining the temporal variations of Ra isotopes and Rn in the groundwater end-member: Implications for derived SGD estimates. *Science of the Total Environment*, *595*, 849–857. https://doi.org/10.1016/j.scitotenv.2017.03.005

Charette, M. A. (2007). Hydrologic forcing of submarine groundwater discharge: Insight from a seasonal study of radium isotopes in a groundwater-dominated salt marsh estuary. *Limnology and Oceanography*, *52*(1), 230–239. https://doi.org/10.4319/lo.2007.52.1.0230

Charette, M. A., & Allen, M. C. (2006). Precision ground water sampling in coastal aquifers using a direct-push, Shielded-Screen Well-Point System. *Groundwater Monitoring & Remediation*, *26*(2), 87–93. https://doi.org/10.1111/j.1745-6592.2006.00076.x

Charette, M. A., Dulaiova, H., Gonneea, M. E., Henderson, P. B., Moore, W. S., Scholten, J. C., et al. (2012). GEOTRACES radium isotopes interlaboratory comparison experiment. *Limnology and Oceanography: Methods*, *10*(6), 451–463. https://doi.org/10.4319/lom.2012.10.451

Chen, Z. Y., Li, K. M., Lin, W. S., & Liu, A. P. (2010). Atmospheric dry and wet deposition of nitrogen and phosphorus in the Pearl River Estuary [in Chinese with English abstract]. *Environmental Pollution & Control*, *32*(11), 53–57. https://doi.org/10.15985/j.cnki.1001-3865.2010.11.014

Cho, H. M., & Kim, G. (2016). Determining groundwater Ra end-member values for the estimation of the magnitude of submarine groundwater discharge using Ra isotope tracers. *Geophysical Research Letters*, *43*, 3865–3871. https://doi.org/10.1002/2016GL068805

Cyronak, T., Santos, I. R., Erler, D. V., Maher, D. T., & Eyre, B. D. (2014). Drivers of pCO_2 variability in two contrasting coral reef lagoons: The influence of submarine groundwater discharge. *Global Biogeochemical Cycles*, *28*, 398–414. https://doi.org/10.1002/2013GB004598

Dai Dyer, K. R., & Taylor, P. A. (1973). A simple, segmented prism model of tidal mixing in well-mixed estuaries. *Estuarine and Coastal Marine Science*, *1*(4), 411–418. https://doi.org/10.1016/0302-3524(73)90030-3

Dai, Z. J., Fagherazzi, S., Mei, X. F., & Gao, J. J. (2016). Decline in suspended sediment concentration delivered by the Changjiang (Yangtze) River into the East China Sea between 1956 and 2013. *Geomorphology*, *268*, 123–132. http://dx.doi.org/10.1016/j.geomorph.2016.06.009

Dai, Z. J., & Liu, J. T. (2013) Impacts of large dams on downstream fluvial sedimentation: An example of the Three Gorges Dam (TGD) on the Changjiang (Yangtze River). *Journal of Hydrology*, *480*, 10–18. http://dx.doi.org/10.1016/j.jhydrol.2012.12.003

Dai, Z. J., Liu, J. T., Wei, W., & Chen, J. Y. (2014). Detection of the Three Gorges Dam influence on the Changjiang (Yangtze River) submerged delta. *Scientific Reports*, *4*, 6600. https://doi.org/10.1038/srep06600

Editorial Board of China Bay Survey. (1993). Guangxi Bay. In S. H. Li & G. Z. Li (Eds.), *Survey of China Bays* (Vol. 12, pp. 144–216) [in Chinese]. Beijing, China: China Ocean Press.

Ferrarin, C., Rapaglia, J., Zaggia, L., Umgiesser, G., & Zuppi, G. M. (2008). Coincident application of a mass balance of radium and a hydrodynamic model for the seasonal quantification of groundwater flux into the Venice Lagoon, Italy. *Marine Chemistry*, *112*(3–4), 179–188. https://doi.org/10.1016/j.marchem.2008.08.008

Galloway, J. N., Townsend, A. R., Erisman, J. W., Bekunda, M., Cai, Z., Freney, J. R., et al. (2008). Transformation of the nitrogen cycle: Recent trends, questions, and potential solutions. *Science*, *320*(5878), 889–892. https://doi.org/10.1126/science.1136674

Garcia-Solsona, E., Garcia-Orellana, J., Masqué, P., Rodellas, V., Mejías, M., Ballesteros, B., et al. (2010). Groundwater and nutrient discharge through karstic coastal springs (Castelló, Spain). *Biogeosciences*, *7*(9), 2625–2638. https://doi.org/10.5194/bg-7-2625-2010

Garcia-Solsona, E., Masqué, P., Garcia-Orellana, J., Rapaglia, J., Beck, A. J., Cochran, J. K., et al. (2008). Estimating submarine groundwater discharge around Isola La Cura, northern Venice Lagoon (Italy), by using the radium quartet. *Marine Chemistry*, *109*(3), 292–306. https://doi.org/10.1016/j.marchem.2008.02.007

Gattacceca, J. C., Mayer, A., Cucco, A., Claude, C., Radakovitch, O., Vallet-Coulomb, C., et al. (2011). Submarine groundwater discharge in a subsiding coastal lowland: A ^{226}Ra and ^{222}Rn investigation in the Southern Venice Lagoon. *Applied Geochemistry*, *26*(5), 907–920. https://doi.org/10.1016/j.apgeochem.2011.03.001

Ge, Z. P., Dai, Z. J., Xie, H. L., Wei, W., Lin, Y. F., & Gao, J. J. (2014). Temporal and spatial characteristics of the shoreline along the Beibu Gulf [in Chinese with English abstract]. *Shanghai Land & Resources*, *35*(2), 49–53. https://doi.org/10.3969/j.issn.2095-1329.2014.02.013

Gonneea, M. E., Charette, M. A., Liu, Q., Herrera-Silveira, J. A., & Morales-Ojeda, S. M. (2014). Trace element geochemistry of groundwater in a karst subterranean estuary (Yucatan Peninsula, Mexico). *Geochimica et Cosmochimica Acta*, *132*, 31–49. https://doi.org/10.1016/j.gca.2014.01.037

Gonneea, M. E., Mulligan, A. E., & Charette, M. A. (2013). Seasonal cycles in radium and barium within a subterranean estuary: Implications for groundwater derived chemical fluxes to surface waters. *Geochimica et Cosmochimica Acta*, *119*, 164–177. https://doi.org/10.1016/j.gca.2013.05.034

Gordon, D. C., Boudreau, P. R., Mann, K. H., Ong, J. E., Silvert, W. L., Smith, S. V., et al. (1996). *LOICZ biogeochemical modelling guidelines* (Vol. 5). LOICZ Core Project. Netherlands Institute for Sea Research.

Gu, H. Q., Moore, W. S., Zhang, L., Du, J. Z., & Zhang, J. (2012). Using radium isotopes to estimate the residence time and the contribution of submarine groundwater discharge (SGD) in the Changjiang effluent plume, East China Sea. *Continental Shelf Research*, *35*, 95–107. https://doi.org/10.1016/j.csr.2012.01.002

Gu, Y. G., Lin, Q., Yu, Z. L., Wang, X. N., Ke, C. L., & Ning, J. J. (2015). Speciation and risk of heavy metals in sediments and human health implications of heavy metals in edible nekton in Beibu Gulf, China: A case study of Qinzhou Bay. *Marine Pollution Bulletin*, *101*(2), 852–859. https://doi.org/10.1016/j.marpolbul.2015.11.019

Guo, Z. R., Ma, Z. Y., Zhang, B., Yuan, X. J., Liu, H. T., & Liu, J. (2013). Tracing submarine groundwater discharge and associated nutrient fluxes into Jiaozhou Bay by continuous ^{222}Rn measurements [in Chinese with English abstract]. *Earth Science-Journal of China University of Geosciences*, *38*(5), 1073–1080. https://doi.org/10.3799/dqkx.2013.105

Hagy, J. D., Boynton, W. R., Keefe, C. W., & Wood, K. V. (2004). Hypoxia in Chesapeake Bay, 1950–2001: Long-term change in relation to nutrient loading and river flow. *Estuaries*, *27*(4), 634–658.

Han, L. J. (2013). *Nutrient characteristics and source apportionment in atmospheric deposition of the Yellow Sea and East China Sea* [in Chinese with English abstract] (China master's thesis). Qingdao, Shandong, China: Ocean University of China.

Harding, L. W., Adolf, J. E., Mallonee, M. E., Miller, W. D., Gallegos, C. L., Perry, E. S., et al. (2015). Climate effects on phytoplankton floral composition in Chesapeake Bay. *Estuarine, Coastal and Shelf Science*, *162*, 53–68. https://doi.org/10.1016/j.ecss.2014.12.030

Hu, C., Muller-Karger, F. E., & Swarzenski, P. W. (2006). Hurricanes, submarine groundwater discharge, and Florida's red tides. *Geophysical Research Letters*, *33*, L11601. https://doi.org/10.1029/2005GL025449

Huang, K. F., You, C. F., Chung, C. H., & Lin, I. T. (2011). Nonhomogeneous seawater Sr isotopic composition in the coastal oceans: A novel tool for tracing water masses and submarine groundwater discharge. *Geochemistry, Geophysics, Geosystems*, *12*, Q05002. https://doi.org/10.1029/2010GC003372

Hwang, D. W., Kim, G., Lee, W. C., & Oh, H. T. (2010). The role of submarine groundwater discharge (SGD) in nutrient budgets of Gamak Bay, a shellfish farming bay, in Korea. *Journal of Sea Research*, *64*(3), 224–230.

Hwang, D. W., Lee, I. S., Choi, M., & Kim, T. H. (2016). Estimating the input of submarine groundwater discharge (SGD) and SGD-derived nutrients in Geoje Bay, Korea using ^{222}Rn-Si mass balance model. *Marine Pollution Bulletin*, *110*(1), 119–126.

Hwang, D. W., Lee, Y. W., & Kim, G. (2005). Large submarine groundwater discharge and benthic eutrophication in Bangdu Bay on volcanic Jeju Island, Korea. *Limnology and Oceanography*, *50*(5), 1393–1403. https://doi.org/10.4319/lo.2005.50.5.1393

Ji, T., Du, J. Z., Moore, W. S., Zhang, G. S., Su, N., & Zhang, J. (2013). Nutrient inputs to a Lagoon through submarine groundwater discharge: The case of Laoye Lagoon, Hainan, China. *Journal of Marine Systems*, *111*, 253–262. https://doi.org/10.1016/j.jmarsys.2012.11.007

Kim, G., Burnett, W. C., Dulaiova, H., Swarzenski, P. W., & Moore, W. S. (2001). Measurement of ^{224}Ra and ^{226}Ra activities in natural waters using a radon-in-air monitor. *Environmental Science & Technology*, *35*(23), 4680–4683. https://doi.org/10.1021/es010804u

Kim, G., & Hwang, D. W. (2002). Tidal pumping of groundwater into the coastal ocean revealed from submarine ^{222}Rn and CH_4 monitoring. *Geophysical Research Letters*, *29*(14), 1678. https://doi.org/10.1029/2002GL015093

Kim, G., Ryu, J. W., & Hwang, D. W. (2008). Radium tracing of submarine groundwater discharge (SGD) and associated nutrient fluxes in a highly-permeable bed coastal zone, Korea. *Marine Chemistry*, *109*(3), 307–317. https://doi.org/10.1016/j.marchem.2007.07.002

King, J. N. (2012). Synthesis of benthic flux components in the Patos Lagoon coastal zone, Rio Grande do Sul, Brazil. *Water Resources Research*, *48*, W12530. https://doi.org/10.1029/2011WR011477

Knight, J. M., Dale, P. E. R., Dunn, R. J. K., Broadbent, G. J., & Lemckert, C. J. (2008). Patterns of tidal flooding within a mangrove forest: Coombabah Lake, Southeast Queensland, Australia. *Estuarine, Coastal and Shelf Science*, *76*(3), 580–593. https://doi.org/10.1016/j.ecss.2007.07.044

Konikow, L. F., Akhavan, M., Langevin, C. D., Michael, H. A., & Sawyer, A. H. (2013). Seawater circulation in sediments driven by interactions between seabed topography and fluid density. *Water Resources Research*, *49*, 1386–1399. https://doi.org/10.1002/wrcr.20121

Lambert, M. J., & Burnett, W. C. (2003). Submarine groundwater discharge estimates at a Florida coastal site based on continuous radon measurements. *Biogeochemistry*, *66*(1/2), 55–73. https://doi.org/10.1023/B:BIOG.0000006057.63478.fa

Lan, W. L., & Peng, X. Y. (2011). Eutrophication status and its impact on phytoplankton biomass in the Maowei Sea [in Chinese with English abstract]. *Journal of Guangxi Academy of Sciences*, *2*, 012. https://doi.org/10.13657/j.cnki.gxkxyxb.2011.02.009

Lapointe, B. E., O'Connell, J. D., & Garrett, G. S. (1990). Nutrient couplings between on-site sewage disposal systems, groundwaters, and nearshore surface waters of the Florida Keys. *Biogeochemistry*, *10*(3), 289–307.

Lee, Y. W., Kim, G., Lim, W., & Hwang, D. W. (2010). A relationship between submarine groundwater borne nutrients traced by Ra isotopes and the intensity of dinoflagellate red-tides occurring in the southern sea of Korea. *Limnology and Oceanography*, *55*(1), 1–10. https://doi.org/10.4319/lo.2010.55.1.0001

Li, S. S., Dai, Z. J., Mei, X. F., Huang, H., Wei, W., & Gao, J. J. (2017). Dramatic variations in water discharge and sediment load from Nanliu River (China) to the Beibu Gulf during 1960s–2013. *Quaternary International*, *440*, 12–23. http://dx.doi.org/10.1016/j.quaint.2016.02.065

Lin, P. (1989). Biomass and element cycle of kandelia forest, China. *Journal of Wuhan Botanical Research*, *7*, 251–257.

Liu, J. A., Du, J. Z., & Yi, L. X. (2017). Ra tracer-based study of submarine groundwater discharge and associated nutrient fluxes into the Bohai Sea, China: A highly human-affected marginal sea. *Journal of Geophysical Research: Oceans*, *122*, 8646–8660. https://doi.org/10.1002/2017JC013095

Liu, S. M., Hong, G. H., Zhang, J., Ye, X. W., & Jiang, X. L. (2009). Nutrient budgets for large Chinese estuaries. *Biogeosciences*, *6*(10), 2245–2263.

Liu, S. M., Zhang, J., Chen, H. T., & Zhang, G. S. (2005). Factors influencing nutrient dynamics in the eutrophic Jiaozhou Bay, North China. *Progress in Oceanography*, *66*(1), 66–85.

Long, Y. X., Tan, X., Han, B. X., Qin, Q. R., & Jiang, Y., Y. (2012). Research on status and sources of nutrients in the Maowei Sea [in Chinese with English abstract]. *Ecological Science*, *31*(5), 572–576. https://doi.org/10.3969/j.issn.1008-8873.2012.05.018

Lu, J. F., Dong, Z. B., Hu, G. Y., Yan, C. Z., Wei, Z. H., & Song, X. (2011). Land use and land cover change and its driving forces in the source region of the Yangtze River during 1990–2005. In *2011 International Symposium on Water Resource and Environmental Protection (ISWREP)* (Vol. 4, pp. 2571–2574). Piscataway, NJ: IEEE.

Luo, X., & Jiao, J. J. (2016). Submarine groundwater discharge and nutrient loadings in Tolo Harbor, Hong Kong using multiple geotracer-based models, and their implications of red tide outbreaks. *Water Research*, *102*, 11–31. https://doi.org/10.1016/j.watres.2016.06.017

MacIntyre, S., Wanninkhof, R., & Chanton, J. P. (1995). Trace gas exchange across the air-water interface in freshwater and coastal marine environments. In R. C. Harris & P. A. Mattson (Eds.), *Biogenic trace gases: Measuring emissions from soil and water* (pp. 52–77). Hoboken, NJ: Blackwell Science.

Martens, C. S., Klump, J. V., & Kipphut, G. W. (1980). Sediment-water chemical exchange in the coastal zone traced by in situ radon-222 flux measurements. *Science*, *208*(4441), 285–288.

McCormack, T., Gill, L. W., Naughton, O., & Johnston, P. M. (2014). Quantification of submarine/intertidal groundwater discharge and nutrient loading from a lowland karst catchment. *Journal of Hydrology*, *519*, 2318–2330. https://doi.org/10.1016/j.jhydrol.2014.09.086

McCoy, C., Viso, R., Peterson, R. N., Libes, S., Lewis, B., Ledoux, J., et al. (2011). Radon as an indicator of limited cross-shelf mixing of submarine groundwater discharge along an open ocean beach in the South Atlantic Bight during observed hypoxia. *Continental Shelf Research*, *31*(12), 1306–1317. https://doi.org/10.1016/j.csr.2011.05.009

Michael, H. A., Charette, M. A., & Harvey, C. F. (2011). Patterns and variability of groundwater flow and radium activity at the coast: A case study from Waquoit Bay, Massachusetts. *Marine Chemistry*, *127*(1), 100–114. https://doi.org/10.1016/j.marchem.2011.08.001

Michael, H. A., Lubetsky, J. S., & Harvey, C. F. (2003). Characterizing submarine groundwater discharge: A seepage meter study in Waquoit Bay, Massachusetts. *Geophysical Research Letters*, *30*(6), 1297. https://doi.org/10.1029/2002GL016000

Moore, W. S. (2003). Sources and fluxes of submarine groundwater discharge delineated by radium isotopes. *Biogeochemistry*, *66*(1/2), 75–93.

Moore, W. S. (2010). The effect of submarine groundwater discharge on the ocean. *Annual Review of Marine Science*, *2*(1), 59–88. https://doi.org/10.1146/annurev-marine-120308-081019

Moore, W. S., Blanton, J. O., & Joye, S. B. (2006). Estimates of flushing times, submarine groundwater discharge, and nutrient fluxes to Okatee Estuary, South Carolina. *Journal of Geophysical Research*, *111*, C09006. https://doi.org/10.1029/2005JC003041

Moore, W. S., & Wilson, A. M. (2005). Advective flow through the upper continental shelf driven by storms, buoyancy, and submarine groundwater discharge. *Earth and Planetary Science Letters*, *235*(3–4), 564–576. https://doi.org/10.1016/j.epsl.2005.04.043

Mwashote, B. M., Murray, M., Burnett, W. C., Chanton, J., Kruse, S., & Forde, A. (2013). Submarine groundwater discharge in the Sarasota Bay system: Its assessment and implications for the nearshore coastal environment. *Continental Shelf Research*, *53*, 63–76. https://doi.org/10.1016/j.csr.2012.12.002

Niencheski, L. F. H., Windom, H. L., Moore, W. S., & Jahnke, R. A. (2007). Submarine groundwater discharge of nutrients to the ocean along a coastal lagoon barrier, Southern Brazil. *Marine Chemistry*, *106*(3), 546–561. https://doi.org/10.1016/j.marchem.2007.06.004

Niu, Y. L. (2014). *Study on several variation of the C, N, P, Si budget of the bivalves in Sungo Bay* [in Chinese with English abstract] (China master's thesis). Zhoushan, China: Zhejiang Ocean University.

Peng, T. H., Takahashi, T., & Broecker, W. S. (1974). Surface radon measurements in the North Pacific Ocean station PAPA. *Journal of Geophysical Research*, *79*(12), 1772–1780. https://doi.org/10.1029/JC079i012p01772

Peterson, R. N., Burnett, W. C., Glenn, C. R., & Johnson, A. G. (2009). Quantification of point-source groundwater discharges to the ocean from the shoreline of the Big Island, Hawaii. *Limnology and Oceanography*, *54*(3), 890–904.

Pilson, M. E. (1998). *An introduction to the chemistry of the sea* (431 pp.). Upper Saddle River, NJ: Prentice Hall.

Rahaman, W., & Singh, S. K. (2012). Sr and ^{87}Sr/^{86}Sr in estuaries of western India: Impact of submarine groundwater discharge. *Geochimica et Cosmochimica Acta*, *85*, 275–288. https://doi.org/10.1016/j.gca.2012.02.025

Rapaglia, J., Ferrarin, C., Zaggia, L., Moore, W. S., Umgiesser, G., Garcia-Solsona, E., et al. (2010). Investigation of residence time and groundwater flux in Venice Lagoon: Comparing radium isotope and hydrodynamical models. *Journal of Environmental Radioactivity*, *101*(7), 571–581. https://doi.org/10.1016/j.jenvrad.2009.08.010

Rapaglia, J., Koukoulas, S., Zaggia, L., Lichter, M., Manfé, G., & Vafeidis, A. T. (2012). Quantification of submarine groundwater discharge and optimal radium sampling distribution in the Lesina Lagoon, Italy. *Journal of Marine Systems*, *91*(1), 11–19. https://doi.org/10.1016/j.jmarsys.2011.09.003

Sadat-Noori, M., Santos, I. R., Sanders, C. J., Sanders, L. M., & Maher, D. T. (2015). Groundwater discharge into an estuary using spatially distributed radon time series and radium isotopes. *Journal of Hydrology*, *528*, 703–719. https://doi.org/10.1016/j.jhydrol.2015.06.056

Sadat-Noori, M., Santos, I. R., Tait, D. R., McMahon, A., Kadel, S., & Maher, D. T. (2016). Intermittently Closed and Open Lakes and/or Lagoons (ICOLLs) as groundwater-dominated coastal systems: Evidence from seasonal radon observations. *Journal of Hydrology*, *535*, 612–624. https://doi.org/10.1016/j.jhydrol.2016.01.080

Sanford, L. P., Boicourt, W. C., & Rives, S. R. (1992). Model for estimating tidal flushing of small embayments. *Journal of Waterway, Port, Coastal, and Ocean Engineering*, *118*(6), 635–654. https://doi.org/10.1061/(ASCE)0733-950X(1992)118:6(635)

Santos, I. R., Beck, M., Brumsack, H. J., Maher, D. T., Dittmar, T., Waska, H., et al. (2015). Porewater exchange as a driver of carbon dynamics across a terrestrial-marine transect: Insights from coupled ^{222}Rn and pCO_2 observations in the German Wadden Sea. *Marine Chemistry*, *171*, 10–20. https://doi.org/10.1016/j.marchem.2015.02.005

Santos, I. R., Burnett, W. C., Dittmar, T., Suryaputra, I. G., & Chanton, J. (2009). Tidal pumping drives nutrient and dissolved organic matter dynamics in a Gulf of Mexico subterranean estuary. *Geochimica et Cosmochimica Acta*, *73*(5), 1325–1339. https://doi.org/10.1016/j.gca.2008.11.029

Santos, I. R., Lechuga-Deveze, C., Peterson, R. N., & Burnett, W. C. (2011). Tracing submarine hydrothermal inputs into a coastal bay in Baja California using radon. *Chemical Geology*, *282*(1), 1–10. https://doi.org/10.1016/j.chemgeo.2010.12.024

Santos, I. R. S., Burnett, W. C., Chanton, J., Mwashote, B., Suryaputra, I. G., & Dittmar, T. (2008). Nutrient biogeochemistry in a Gulf of Mexico subterranean estuary and groundwater-derived fluxes to the coastal ocean. *Limnology and Oceanography*, *53*(2), 705–718. https://doi.org/10.4319/lo.2008.53.2.0705

Slomp, C. P., & Van Cappellen, P. (2004). Nutrient inputs to the coastal ocean through submarine groundwater discharge: Controls and potential impact. *Journal of Hydrology*, *295*(1), 64–86. https://doi.org/10.1016/j.jhydrol.2004.02.018

Smith, C. G., Cable, J. E., Martin, J. B., & Roy, M. (2008). Evaluating the source and seasonality of submarine groundwater discharge using a radon-222 pore water transport model. *Earth and Planetary Science Letters*, *273*(3), 312–322. https://doi.org/10.1016/j.epsl.2008.06.043

Su, N., Du, J. Z., Moore, W. S., Liu, S. M., & Zhang, J. (2011). An examination of groundwater discharge and the associated nutrient fluxes into the estuaries of eastern Hainan Island, China using ^{226}Ra. *Science of the Total Environment*, *409*(19), 3909–3918. https://doi.org/10.1016/j.scitotenv.2011.06.017

Sugimoto, R., Honda, H., Kobayashi, S., Takao, Y., Tahara, D., Tominaga, O., et al. (2016). Seasonal changes in submarine groundwater discharge and associated nutrient transport into a tideless semi-enclosed embayment (Obama Bay, Japan). *Estuaries and Coasts*, *39*(1), 13–26. https://doi.org/10.1007/s12237-015-9986-7

Swarzenski, P. W., Reich, C., Kroeger, K. D., & Baskaran, M. (2007). Ra and Rn isotopes as natural tracers of submarine groundwater discharge in Tampa Bay, Florida. *Marine Chemistry*, *104*(1), 69–84. https://doi.org/10.1016/j.marchem.2006.08.001

Szymczycha, B., Vogler, S., & Pempkowiak, J. (2012). Nutrient fluxes via submarine groundwater discharge to the Bay of Puck, southern Baltic Sea. *Science of the Total Environment*, *438*, 86–93. https://doi.org/10.1016/j.scitotenv.2012.08.058

Taniguchi, M., Burnett, W. C., Cable, J. E., & Turner, J. V. (2002). Investigation of submarine groundwater discharge. *Hydrological Processes*, *16*(11), 2115–2129. https://doi.org/10.1002/hyp.1145

Taniguchi, M., Burnett, W. C., Dulaiova, H., Kontar, E. A., Povinec, P. P., & Moore, W. S. (2006). Submarine groundwater discharge measured by seepage meters in Sicilian coastal waters. *Continental Shelf Research*, *26*(7), 835–842. https://doi.org/10.1016/j.csr.2005.12.002

Taniguchi, M., Ishitobi, T., & Saeki, K. I. (2005). Evaluation of time-space distributions of submarine ground water discharge. *Ground Water*, *43*(3), 336–342. https://doi.org/10.1111/j.1745-6584.2005.0027.x

Tian, H. T., Hu, X. S., Zhang, S. F., Xie, J., Zhang, D., & An, J. S. (2014). Distribution and potential ecological risk assessment of heavy metals in surface sediments of Maowei Sea [in Chinese with English abstract]. *Marine Environmental Science*, *33*, 187–191.

Townsend, A. R., Howarth, R. W., Bazzaz, F. A., Booth, M. S., Cleveland, C. C., Collinge, S. K., et al. (2003). Human health effects of a changing global nitrogen cycle. *Frontiers in Ecology and the Environment*, *1*(5), 240–246. https://doi.org/10.1890/1540-9295(2003)001[0240:HHEOAC]2.0.CO;2

Tse, K. C., & Jiao, J. J. (2008). Estimation of submarine groundwater discharge in plover cove, Tolo harbour, Hong Kong by ^{222}Rn. *Marine Chemistry*, *111*(3), 160–170. https://doi.org/10.1016/j.marchem.2008.04.012

Ullman, W. J., & Aller, R. C. (1982). Diffusion coefficients in nearshore marine sediments. *Limnology and Oceanography*, *27*(3), 552–556. https://doi.org/10.4319/lo.1982.27.3.0552

Urquidi-Gaume, M., Santos, I. R., & Lechuga-Deveze, C. (2016). Submarine groundwater discharge as a source of dissolved nutrients to an arid coastal embayment (La Paz, Mexico). *Environmental Earth Sciences*, *75*(2), 154. https://doi.org/10.1007/s12665-015-4891-8

Wang, G., Jing, W., Wang, S., Xu, Y., Wang, Z., Zhang, Z., et al. (2014). Coastal acidification induced by tidal-driven submarine groundwater discharge in a coastal coral reef system. *Environmental Science & Technology*, *48*(22), 13069–13075. https://doi.org/10.1021/es5026867

Wang, G. Z., Wang, Z. Y., Zhai, W. D., Moore, W. S., Li, Q., Yan, X. L., et al. (2015). Net subterranean estuarine export fluxes of dissolved inorganic C, N, P, Si, and total alkalinity into the Jiulong River estuary, China. *Geochimica et Cosmochimica Acta*, *149*, 103–114. https://doi.org/10.1016/j.gca.2014.11.001

Wang, X., Li, H., Jiao, J. J., Barry, D. A., Li, L., Luo, X., et al. (2015). Submarine fresh groundwater discharge into Laizhou Bay comparable to the Yellow River flux. *Scientific Reports*, *5*(1), 8814. https://doi.org/10.1038/srep08814

Wang, X., Li, H., Yang, J., Zheng, C., Zhang, Y., An, A., et al. (2017). Nutrient inputs through submarine groundwater discharge in an embayment: A radon investigation in Daya Bay, China. *Journal of Hydrology*, *551*, 784–792. https://doi.org/10.1016/j.jhydrol.2017.02.036

Wang, X. L. (2017). *Study on submarine groundwater discharge (SGD) and its driven nutrient fluxes from typical water area in coastal sea of China* [in Chinese with English abstract] (China doctoral dissertation). Shanghai, China: East China Normal University.

Wang, X. L., & Du, J. Z. (2016). Submarine groundwater discharge into typical tropical lagoons: A case study in eastern Hainan Island, China. *Geochemistry, Geophysics, Geosystems*, *17*, 4366–4382. https://doi.org/10.1002/2016GC006502

Wang, X. L., Du, J. Z., Ji, T., Wen, T. Y., Liu, S. M., & Zhang, J. (2014). An estimation of nutrient fluxes via submarine groundwater discharge into the Sanggou Bay—A typical multi-species culture ecosystem in China. *Marine Chemistry*, *167*, 113–122. https://doi.org/10.1016/j.marchem.2014.07.002

Wang, Y. H. (2013). *Numerical modeling tidal circulation and morphodynamics in a dumbbell-shaped coastal embayment*. INTECH Open Access Publisher. https://doi.org/10.5772/51760

Wang, Y. H., Yang, X. L., Lv, Z. B., Zhang, H. J., Li, F., & Yang, J. M. (2008). Abundance of nano-phytoplankton and the relation to nutrient in the inshore of Shandong [in Chinese with English abstract]. *Oceanologia Limnologia Sinica*, *39*, 643–649.

Waska, H., & Kim, G. (2011). Submarine groundwater discharge (SGD) as a main nutrient source for benthic and water-column primary production in a large intertidal environment of the Yellow Sea. *Journal of Sea Research*, *65*(1), 103–113. https://doi.org/10.1016/j.seares.2010.08.001

Wei, M. X., & He, B. M. (2008). Change trend of water environmental index in last 20 a of Qinzhou Bay V. Biomass distribution of phytoplankton and effect factors [in Chinese with English abstract]. *Marine Environmental Science*, *27*(3), 253–257.

Wei, M. X., Lai, T. H., & He, B. M. (2002). Change trend of the chemical items in Qinzhou Bay in the last twenty years. I. Nutrient condition in usual discharged period [in Chinese with English abstract]. *Marine Environmental Science*, *21*(3), 49–52.

Wen, T. Y., Du, J. Z., Ji, T., Wang, X. L., & Deng, B. (2014). Use of ^{222}Rn to trace submarine groundwater discharge in a tidal period along the coast of Xiangshan, Zhejiang, China. *Journal of Radioanalytical and Nuclear Chemistry*, *299*(1), 53–60. https://doi.org/10.1007/s10967-013-2786-2

Wu, J. X. (2005). *Development and applications of dynamic model for dissolved nitrogen and phosphate budgets in Sungo Bay* [in Chinese with English abstract] (China master's thesis). Qingdao, Shandong, China: Ocean University of China.

Wu, W. C., Ren, L. L., Cai, X. D., & Wang, T. (2014). Spatial pattern and ecological risk of heavy metals in sediments from Maowei Sea, Southern China [in Chinese with English abstract]. *Research of Environmental Sciences*, *27*(2), 147–156. https://doi.org/13198/j.issn.1001-6929.2014.02.06

Wu, Z. J., Zhou, H. Y., Zhang, S., & Liu, Y. (2013). Using ^{222}Rn to estimate submarine groundwater discharge (SGD) and the associated nutrient fluxes into Xiangshan Bay, East China Sea. *Marine Pollution Bulletin*, *73*(1), 183–191. https://doi.org/10.1016/j.marpolbul.2013.05.024

Xia, D., Yu, Z. G., Xu, B. C., Gao, M. S., Mi, T. Z., Jiang, X. Y., et al. (2016). Variations of hydrodynamics and submarine groundwater discharge in the Yellow River estuary under the influence of the water-sediment regulation scheme. *Estuaries and Coasts*, *39*(2), 333–343. https://doi.org/10.1007/s12237-015-9994-7

Yang, B., Fang, H. Y., Zong, Q. P., Zhang, C. X., & Li, S. P. (2012). Distribution characteristics of nutrients and eutrophication assessment in summer in Qinzhou Bay [in Chinese with English abstract]. *Marine Sciences Bulletin*, *31*(16), 640–645.

Yang, B., Zong, Q. P., Zhang, C. X., Lu, D. L., Liang, Y. R., & Li, S. P. (2015). Spatio-temporal variations of chlorophyll *a* and primary productivity and its influence factors in Qinzhou Bay [in Chinese with English abstract]. *Acta Scientiae Circumstantiae*, *35*(5), 1333–1340. https://doi.org/10.13671/j.hjkxxb.2014.0902

Zhang, J. L., Li, Y. Y., Wang, Y. H., Zhang, Y. Y., Zhang, D., Zhang, R. J., et al. (2014). Spatial distribution and ecological risk of polychlorinated biphenyls in sediments from Qinzhou Bay, Beibu Gulf of South China. *Marine Pollution Bulletin*, *80*(1), 338–343. https://doi.org/10.1016/j.marpolbul.2013.12.028

Zhang, Y., Li, H. L., Wang, X. J., Zheng, C. M., Wang, C. Y., Xiao, K., et al. (2016). Estimation of submarine groundwater discharge and associated nutrient fluxes in eastern Laizhou Bay, China using ^{222}Rn. *Journal of Hydrology*, *533*, 103–113. https://doi.org/10.1016/j.jhydrol.2015.11.027

Zhao, X. Q. (2011). *The study of bay integrated renovation—Take a Maoweihai for example* [in Chinese with English abstract] (China master's thesis). Xiamen, China: Third Institute of Oceanography, State Oceanic Administration.

Zheng, Q., Zhang, R. J., Wang, Y. H., Pan, X. H., Tang, J. H., & Zhang, G. (2012). Occurrence and distribution of antibiotics in the Beibu Gulf, China: Impacts of river discharge and aquaculture activities. *Marine Environmental Research*, *78*, 26–33. https://doi.org/10.1016/j.marenvres.2012.03.007

Zhu, Y. M. (2011). *Nutrients in atmospheric deposition of the Yellow and East China Sea* [in Chinese with English abstract] (China master's thesis). Qingdao, Shandong, China: Ocean University of China.

Zhuang, J. L., Jiang, F. J., Xu, M. B., Zhang, R. C., Wang, Y. B., Ke, K., et al. (2012). Annual change of environmental factors and phytoplankton community characteristics in Maowei Sea of Qinzhou Bay [in Chinese with English abstract]. *Guangxi Sciences*, *19*(3), 263–267. https://doi.org/10.13656/j.cnki.gxkx.2012.03.010

Zou, W., Wang, H. Y., & Gao, J. L. (2011). Fluxes of N and P into Daya bay by atmospheric deposition [in Chinese with English abstract]. *Marine Environmental Science*, *30*(6), 843–846.